

Adaptive domain decomposition method for time-dependent problems with applications in fluid dynamics

Vít Dolejš^a, Jakub Šístek^b

^aCharles University, Faculty of Mathematics and Physics, Sokolovská 83, 186 75 Praha, Czech Republic

^bInstitute of Mathematics of the Czech Academy of Sciences, Žitná 25, 110 00 Praha, Czech Republic

Abstract

We deal with the numerical solution of the time-dependent partial differential equations using the adaptive space-time discontinuous Galerkin (DG) method. The discretization leads to a nonlinear algebraic system at each time level, the size of the system is varying due to mesh adaptation. A Newton-like iterative solver leads to a sequence of linear algebraic systems which are solved by GMRES solver with a domain decomposition preconditioner. Particularly, we consider additive and hybrid two-level Schwarz preconditioners which are efficient and easy to implement for DG discretization. We study the convergence of the linear solver in dependence on the number of subdomains and the number of element of the coarse grid. We propose a simplified cost model measuring the computational costs in terms of floating-point operations, the speed of computation, and the wall-clock time for communications among computer cores. Moreover, the cost model serves as a base of the presented adaptive domain decomposition method which chooses the number of subdomains and the number of element of the coarse grid in order to minimize the computational costs. The efficiency of the proposed technique is demonstrated by two benchmark problems of compressible flow simulations.

Keywords: space-time discontinuous Galerkin method, domain decomposition, two-level Schwarz methods, anisotropic hp -mesh adaptation, compressible Navier-Stokes equation, numerical study

2000 MSC: 65M60, 65M50, 76M10

1. Introduction

Numerical solution of time-dependent partial differential equations is an important tool in many areas of science and engineering. Among various numerical techniques, the *space-time discontinuous Galerkin* (STDG) method presents a very powerful discretization approach. It is based on piece-wise polynomial discontinuous approximation with respect to spatial and temporal variables. The main advantages of STDG method are stability, accuracy and robustness, the ability to deal with hp -mesh adaptation, the use of arbitrary non-nested meshes for time-dependent problems, and a relative simplicity of constructing domain decomposition preconditioners. We refer to earlier papers [29, 30, 35, 42] dealing with numerical solution of fluid dynamics problems, [41] using STDG method for the solution of Hamilton–Jacobi–Hellman equations, [9] analysing STDG method for parabolic problems on prismatic meshes, [46] for solving linear transport problem, or [12] dealing with symmetric Friedrichs systems. Papers [21, 22, 37, 44] also present related research. Main theoretical results can be found in [15, Chapter 6].

Numerical solution of time-dependent problems typically involves re-meshing during the evolution process in order to balance the accuracy and efficiency of the simulation. In [14, 18], we developed the *anisotropic hp -mesh adaptation* technique which allows to adapt the size, shape, and orientation of triangular elements together with varying polynomial approximation degrees. This adaptive technique minimizes the number of degrees of freedom so that an interpolation error estimate is under the given tolerance. The STDG method naturally handles grids generated by the anisotropic mesh adaptation method since it is a one-step method, and the approximate solutions at different time

Email addresses: vit.dolejsi@matfyz.cuni.cz (Vít Dolejš), sistek@math.cas.cz (Jakub Šístek)

levels are connected only weakly by a time penalty term. The computational benefit of anisotropic mesh adaptation for unsteady flow problems was presented in many papers, e.g., [1, 7, 20, 24, 38] and the references cited therein.

The significant disadvantage of STDG method is the size of the arising nonlinear algebraic systems. Particularly, using the approximation of degree $q \geq 0$, STDG method gives a system of size $(q+1) \times \text{DoF}$ at each time step where DoF is the number of spatial degrees of freedom. The temporal accuracy of this scheme at the nodes of the time partition is $2q+1$. On the other hand, the popular diagonally implicit Runge-Kutta (DIRK) methods ([2, 8, 10, 25, 31, 40]) having order $r \geq 1$ require the solution of r systems of size DoF at each time step which is typically faster. Therefore, to make the STDG approach competitive, efficient algebraic solvers are required.

The iterative solution of nonlinear algebraic systems leads to sequences of linear systems that are frequently solved iteratively by Krylov methods [32] with suitable preconditioners. A prominent role is played by the *domain decomposition* (DD) techniques [13, 45] since they can employ the power of parallel computers. Their combination with discontinuous Galerkin discretization leads to a very comfortable setting. Namely, non-overlapping domain decomposition preconditioners do not require any special choice of the interface conditions among subdomains. Furthermore, two-level Schwarz preconditioners, which accelerate the transfer of information through the whole system, can be constructed in a natural way, see e.g., [5, 6, 19, 27].

In this paper, we employ a domain decomposition preconditioners for the solution of systems arising from adaptive STDG discretization of time-dependent partial differential equations describing the motion of fluids. In particular, we adopt additive and hybrid two-level Schwarz techniques with two domain decomposition parameters: the number of subdomains M and the number of elements of the coarse grid n_0 . We note that the subdomains arise from re-grouping of the mesh elements into M connected subdomains by standard tools like METIS [28] such that the number of degrees of freedom of each subdomain is equilibrated. Moreover, the coarse mesh arises from the splitting of each subdomains into s coarse macro-elements, hence the coarse mesh has $n_0 = s \times M$ elements.

It is known and documented also in this paper, that larger M allows to use more parallelization but decreases the speed of convergence. Similarly, a finer coarse mesh provides more information and accelerates the convergence but the corresponding system is larger and, therefore, more expensive to solve. In this paper we consider the following question: How to choose the number of subdomains M and the coarse mesh factor s in an optimal way?

In order to easily analyse the computational costs, we introduce a new *computational cost model* measuring the number of floating point operations (*flops*) per one core, the performance (speed of computation), and the wall-clock time of communications among computer cores. We study numerically, how these costs depend on the domain decomposition parameters M and s . This is the first novelty of this paper. Moreover, based on the computational cost model, we propose an adaptive technique which estimate the computational costs a priori and sets the optimal parameters M and s for domain decomposition. The efficiency of this technique is demonstrated by several numerical experiments. The proposed framework can be applied to an arbitrary adaptive method solving any time-dependent problem. We emphasise that the goal of this paper is not to study and demonstrate the scalability of the preconditioners, but to develop a strategy for choosing optimally the domain decomposition parameters for a particular problem.

In Section 2, we present the model describing the motion of viscous compressible fluid, its discretization by the STDG method with several solution strategies is briefly given in Section 3. The domain decomposition (DD) based preconditioners are explained in Section 4 where we also formulate the fundamental problem of this paper. In Section 5, we discuss the computational costs of the DD preconditioners. The dependence of the computational costs on DD parameters M and s is studied numerically. Moreover, we present the resulting adaptive domain decomposition technique in Section 6, its efficiency is demonstrated by two examples in Section 7, and we conclude with several remarks in Section 8.

2. Governing equations

We consider the system of the compressible Navier-Stokes equations with state equation for perfect gas. Let $\Omega \subset \mathbb{R}^2$ be the computational domain occupied by the fluid, $T > 0$ the physical time to be reached, and $Q_T := \Omega \times (0, T)$. Moreover, the symbols ∂_t and ∂_{x_i} denote the partial derivatives with respect to t and x_i , $i = 1, 2$, respectively. Then the motion of the fluid is described by the system of $n = 4$ convection-diffusion equations

$$\partial_t w + \sum_{i=1}^2 \partial_{x_i} (f_i(w) - R_i(w, \nabla w)) = G(w) \quad \text{in } Q_T, \quad (1)$$

where $w = w(x, t) : Q_T \rightarrow \mathbb{R}^n$ is the unknown state vector, $f_i : \mathbb{R}^n \rightarrow \mathbb{R}^n$, $i = 1, 2$ represent the convective fluxes, $R_i : \mathbb{R}^n \rightarrow \mathbb{R}^n$, $i = 1, 2$ represent the diffusive fluxes, and $G : Q_T \rightarrow \mathbb{R}^n$ denotes the exterior forces. System (1) is accompanied by the initial and boundary conditions. Particularly, we set $w(x, 0) = w_0(x)$ in Ω , where w_0 is a given function. Moreover, various problem-dependent boundary conditions are prescribed on the boundary $\Gamma := \partial\Omega$. The state vector and the fluxes read

$$w = (\rho, \rho v_1, \rho v_2, e)^T, \quad f_i = (\rho v_i, \rho v_i v_1 + \delta_{i1} p, \rho v_i v_2 + \delta_{i2} p, (e + p) v_i)^T, \quad i = 1, 2, \quad (2)$$

$$R_i = \left(0, \tau_{i1}, \tau_{i2}, \sum_{k=1}^2 \tau_{ik} v_i + \frac{\tilde{\mu} c_p}{\text{Pr}} \partial_{x_i} \theta \right)^T, \quad i = 1, 2, \quad G = (0, -\rho g k_1, -\rho g k_2, -\rho g \mathbf{k} \cdot \mathbf{v})^T,$$

where ρ is the density, p is the pressure, $\mathbf{v} = (v_1, v_2)^T$ is the velocity vector, θ is the absolute temperature and $e = \rho c_v \theta + \rho |\mathbf{v}|^2/2$ is the energy per unit volume including the interior and kinetic energies (and excluding the gravitational energy). Moreover, $c_v > 0$ and $c_p > 0$ are the specific heat capacities at constant volume and pressure, respectively, $\kappa = c_p/c_v > 1$ is the Poisson adiabatic constant, $R = c_p - c_v$ is the gas constant, $\tilde{\mu}$ is the dynamic viscosity, $g = 9.81 \text{ m} \cdot \text{s}^{-2}$ is the gravity constant, $\mathbf{k} = (k_1, k_2)^T$ is the upward pointing unit vector, Pr is the Prandtl number, and τ_{ij} , $i, j = 1, 2$ denote the components of the viscous part of the stress tensor. Symbol δ_{ij} is the Kronecker delta and the symbol \cdot denotes the scalar product. The relations (1) – (2) are accompanied by the constitutive relations of the perfect gas and the viscous part of the stress tensor as

$$p = R\rho\theta \quad \text{and} \quad \tau_{ij} = \tilde{\mu} \left(\partial_{x_j} v_i + \partial_{x_i} v_j \right) - \frac{2}{3} \delta_{ij} \left(\partial_{x_1} v_1 + \partial_{x_2} v_2 \right), \quad i, j = 1, 2, \quad \text{respectively.} \quad (3)$$

The efficiency of the presented domain decomposition techniques is demonstrated also on a two-dimensional non-hydrostatic mesoscale atmospheric modeling problem where the preferred physical quantity is the potential temperature Θ given as

$$\Theta = \theta/P, \quad \text{where} \quad P = (p/p_0)^{(\kappa-1)/\kappa} \quad (4)$$

is the Exner pressure, and $p_0 = 10^5 \text{ Pa}$ is the reference pressure. The initial condition is typically set as a perturbation in terms of the potential temperature of a steady-state flow where the mean values $\bar{\Theta}$ and \bar{P} of the Exner pressure and the potential temperature are in a hydrostatic balance (cf. [23]), i.e.,

$$c_p \bar{\Theta} \frac{d\bar{P}}{dx_2} = -g. \quad (5)$$

3. Discontinuous Galerkin discretization

We discretize problem (1) by the *space-time discontinuous Galerkin method*. A detailed description of the method can be found, e.g., in [15, Chapters 8–9] or [14]. Here, we present only the final formulas for completeness.

3.1. Function spaces

We introduce a partition of $(0, T)$ by $0 = t_0 < t_1 < \dots < t_r = T$ and set $I_m = (t_{m-1}, t_m)$, and $\tau_m = t_m - t_{m-1}$ for $m = 1, \dots, r$. For each t_m , $m = 0, \dots, r$, we consider a mesh $\mathcal{T}_{h,m}$ consisting of a finite number of closed triangles K with mutually disjoint interiors and covering $\bar{\Omega}$. The meshes $\mathcal{T}_{h,m}$ can differ for $m = 0, \dots, r$. For each $K \in \mathcal{T}_{h,m}$, $m = 0, \dots, r$, we assign a polynomial approximation degree with respect to space $p_K \geq 1$. Moreover, let $q \geq 0$ be the polynomial approximation degree with respect to time which is constant for all elements. We define the spaces of *discontinuous piecewise polynomial* functions on the space-time layer $\Omega \times I_m$ by

$$S_m^{h,\tau} := \left\{ \psi : \Omega \times I_m \rightarrow \mathbb{R}^n; \psi(x, t)|_{K \times I_m} = \sum_{j=0}^q t^j \varphi(x), \varphi|_K \in [P_{p_K}(K)]^n, K \in \mathcal{T}_{h,m} \right\}, \quad m = 0, \dots, r, \quad (6)$$

where $[P_{p_K}(K)]^n$ denotes the vector-valued space of all polynomials on K of degree $\leq p_K$, $K \in \mathcal{T}_{h,m}$.

To proceed to an algebraic representation, a suitable basis of $S_m^{h,\tau}$ has to be chosen. In the context of discontinuous Galerkin discretization, it is natural to choose the basis functions having support restricted to only one space-time

element $K \times I_m$, $K \in \mathcal{T}_{h,m}$, $m = 1, \dots, r$. Therefore, we consider the basis of the space $S_m^{h,\tau}$, $m = 1, \dots, r$,

$$\mathcal{B}_{h,m} := \{\psi_{\alpha}, \alpha \in B_{h,m}\}, \text{ where } B_{h,m} := \{\alpha; \alpha = \{K, k, i, j\}, j = 0, \dots, q, i = 1, \dots, d_K, k = 1, \dots, n, K \in \mathcal{T}_{h,m}\} \quad (7)$$

is the set of multi-indices α , index i corresponds to the spatial degrees of freedom $1, \dots, d_K := (p_K + 1)(p_K + 2)/2$ (= dimension of $P_{p_K}(K)$), index j corresponds to temporal degrees of freedom $0, \dots, q$, index $k = 1, \dots, n$ denotes the equation and $K \in \mathcal{T}_{h,m}$ is the mesh element. Obviously, the cardinality of set $B_{h,m}$ is equal to $N_m = \dim S_m^{h,\tau}$, cf. (14). Moreover, we denote by $K_{\alpha} \in \mathcal{T}_h$ the element defining multi-index $\alpha \in B_{h,m}$. Then any basis function $\psi_{\alpha}, \alpha \in \mathcal{B}_{h,m}$ has support restricted only to element $K_{\alpha} \in \mathcal{T}_{h,m}$, $m = 1, \dots, r$.

3.2. Space semi-discretization

To derive the space discontinuous Galerkin (DG) semi-discretization, we multiply (1), by $\psi \in S_m^{h,\tau}$, integrate over $K \in \mathcal{T}_{h,m}$, apply Green's theorem, sum over all $K \in \mathcal{T}_{h,m}$, approximate the convective and diffusive fluxes through element boundaries, and add stabilization terms vanishing for any smooth solution w . Then, we obtain an abstract identity

$$(\partial_t w(\cdot, t), \psi(\cdot, t))_{\Omega} + a_{h,m}(w(\cdot, t), \psi(\cdot, t)) = 0 \quad \forall \psi \in S_m^{h,\tau}, \quad t \in I_m, \quad m = 1, \dots, r, \quad (8)$$

where $(\cdot, \cdot)_{\Omega}$ denotes the $L^2(\Omega)$ -scalar product and $a_{h,m}$ is a form arising from DG discretization of (1). This form is linear with respect to its second argument. We refer to [15, Chapters 8–9] or [14] for the particular form of $a_{h,m}$. We only note here that it contains integral over elements $K \in \mathcal{T}_{h,m}$ and their edges.

To treat the nonlinearity of system (8), we introduce its linearized form

$$a_{h,m}^L(\bar{w}, w, \psi) \approx \frac{D}{Dw} a_{h,m}(\bar{w}, \psi) \quad (9)$$

where $\frac{D}{Dw} a_{h,m}(\bar{w}, \psi)$ denotes the Fréchet derivative of $a_{h,m}$ with respect to w evaluated at \bar{w} . It can be derived directly by the differentiation of $a_{h,m}$, or a suitable approximation can be used too, see the references mentioned above. Obviously, a_h^L is linear with respect to its second and third arguments.

3.3. Full space-time discretization

To define the full space-time DG discretization of (1), we integrate (8) over I_m and add a “time-stabilization” terms vanishing for solution continuous with respect to time. Particularly, we introduce the forms

$$\begin{aligned} A_{h,m}(w, \psi) &:= \int_{I_m} \left((\partial_t w, \psi)_{\Omega} + a_{h,m}(w, \psi) \right) dt + (\{w\}_{m-1}, \psi|_{m-1}^+)_{\Omega}, \\ A_{h,m}^L(\bar{w}, w, \psi) &:= \int_{I_m} \left((\partial_t w, \psi)_{\Omega} + a_{h,m}^L(\bar{w}, w, \psi) \right) dt + (w|_{m-1}^+, \psi|_{m-1}^+)_{\Omega}, \quad \bar{w}, w, \psi \in S^{h\tau}, \quad m = 1, \dots, r, \end{aligned} \quad (10)$$

where $S^{h\tau}$ is the function space over the whole space-time cylinder $\Omega \times (0, T)$ given by

$$S^{h\tau} := \{w_{h\tau} \in L^2(\Omega \times (0, T)), w_{h\tau}|_{\Omega \times I_m} =: w_{h\tau}^m \in S_m^{h,\tau}, m = 1, \dots, r\}. \quad (11)$$

The symbol $\{\cdot\}_{m-1}$ in (10) denotes the jump with respect to time on the time level t_m , $m = 0, \dots, r-1$, namely

$$\{\psi\}_m := \psi|_m^+ - \psi|_m^-, \quad \psi|_m^{\pm} := \lim_{\epsilon \rightarrow 0^{\pm}} \psi(t_m + \epsilon), \quad \psi \in S^{h\tau}, \quad (12)$$

where $\psi|_0^-$ is typically taken from the initial condition. The term $(\{w\}_{m-1}, \psi|_m^+)_\Omega$ in (10) joins together the solution on time intervals I_{m-1} and I_m , and it represents the “time penalty”. This term is applicable also for $S_{m-1}^{h,\tau} \neq S_m^{h,\tau}$ which is advantageous for varying meshes during the adaptation process. Form $A_{h,m}^L$ is linear with respect to its second and third arguments. Due to the choice of basis (7), term $A_{h,m}^L(\bar{w}, \psi_{\beta}, \psi_{\alpha})$ for $\psi_{\alpha}, \psi_{\beta} \in S_m^{h,\tau}$ is non-vanishing if $K_{\alpha} = K_{\beta}$ or K_{α} and K_{β} have a common edge. For a detailed derivation of time DG discretization, including the numerical analysis, we refer to [15, Chapter 6].

Now, we formulate the final numerical scheme.

Definition 3.1. We say that the function $w_{h\tau} = \{w_{h\tau}^m, m = 1, \dots, r\} \in S^{h\tau}$ (cf. (11)) is the *space-time discontinuous Galerkin* (STDG) solution of (1) if

$$A_{h,m}(w_{h\tau}, \psi_h) = 0 \quad \forall \psi_h \in S_m^{h,\tau}, \quad m = 1, \dots, r, \quad (13)$$

where we set $w_{h\tau}|_0^- := w_0$ (= the initial condition).

3.4. Solution strategy

For any $m = 1, \dots, r$, formula (13) represents the system of N_m algebraic equations,

$$N_m = \dim S_m^{h,\tau} = (q+1)n \sum_{K \in \mathcal{T}_{h,m}} d_K, \quad d_K = (p_K+1)(p_K+2)/2, \quad K \in \mathcal{T}_{h,m}, \quad (14)$$

for the solution $w_{h\tau}^m \in S_m^{h,\tau}$ (depending also on $w_{h\tau}^{m-1}$). Let $\xi^m \in \mathbb{R}^{N_m}$ be the algebraic representation of $w_{h\tau}^m$ in basis $\mathcal{B}_{h,m}$, cf. (7). Then the algebraic representation of (13) is written as

$$\mathbf{f}_m(\xi^m) = 0, \quad \text{where } \mathbf{f}_m : \mathbb{R}^{N_m} \rightarrow \mathbb{R}^{N_m}, \quad \mathbf{f}_m = \{(\mathbf{f}_m)_{\alpha}\}_{\alpha \in \mathcal{B}_{h,m}}, \quad (\mathbf{f}_m)_{\alpha} = A_{h,m}(w_{h\tau}^m, \psi_{\alpha}), \quad (15)$$

where $\psi_{\alpha} \in \mathcal{B}_{h,m}$ is the basis function. Similarly, let matrix $\mathbf{A}_m(\bar{\xi})$ be the algebraic representation of $A_{h,m}^L(\bar{w}, \cdot, \cdot)$, where $\bar{\xi}$ is the representation of \bar{w} . Namely

$$\mathbf{A}_m : \mathbb{R}^{N_m} \rightarrow \mathbb{R}^{N_m \times N_m}, \quad \mathbf{A}_m(\bar{\xi}) = \{(\mathbf{A}_m(\bar{\xi}))_{\alpha\beta}\}_{\alpha, \beta \in \mathcal{B}_{h,m}}, \quad (\mathbf{A}_m(\bar{\xi}))_{\alpha\beta} = A_{h,m}^L(\bar{w}, \psi_{\beta}, \psi_{\alpha}). \quad (16)$$

In virtue of (9), matrix \mathbf{A}_m is an approximation of the Jacobian of \mathbf{f}_m . Then the damped Newton-like method, computing an approximation of ξ^m by the sequence ξ_{ℓ}^m , $\ell = 0, 1, \dots$, reads

$$\xi_{\ell}^m := \xi_{\ell-1}^m - \lambda_{\ell} \mathbf{d}_{\ell}, \quad \ell = 1, 2, \dots, \quad (17a)$$

$$\text{where } \mathbf{d}_{\ell} \in \mathbb{R}^{N_m} \text{ solves } \mathbf{A}_m(\xi_{\ell-1}^m) \mathbf{d}_{\ell} = \mathbf{f}_m(\xi_{\ell-1}^m), \quad (17b)$$

the initial guess ξ_0^m is taken from the previous time layer, i.e., $\xi_0^m := \xi^{m-1}$, and $0 < \lambda_{\ell} \leq 1$ is the damping parameter. It is chosen based on the monitoring function ζ_{ℓ} given by

$$\zeta_{\ell} := \|\mathbf{f}_m(\xi_{\ell}^m)\|_2 / \|\mathbf{f}_m(\xi_{\ell-1}^m)\|_2, \quad \ell = 1, 2, \dots, \quad (18)$$

where $\|\cdot\|_2$ is the Euclidean norm in \mathbb{R}^{N_m} . For each iteration step ℓ , we solve system (17b) and perform step (17a) with $\lambda_{\ell} = 1$. If $\zeta_{\ell} < 1$, this step is accepted and we proceed to $\ell + 1$. If $\zeta_{\ell} \geq 1$, we reduce λ_{ℓ} by a factor smaller than 1 (0.65 in our case) and repeat step (17a) until $\zeta_{\ell} < 1$. The whole iterative process (17) is stopped when a suitable stopping criterion is achieved, cf. Section 3.5. In the following, we call (17) the *Newton method* for simplicity although its various modification can be considered.

Remark 3.2. The most time consuming parts of the computational process are the evaluation of entries of matrix \mathbf{A}_m in (17b) and, especially, the solution of (17b). To reduce the computational costs, we do not update matrix $\mathbf{A}_m(\xi_{\ell-1}^m)$ for each ℓ since it serves only as an approximation of the Jacobian in the Newton method. In particular, if the monitoring function $\zeta_{\ell} < 1/2$, we keep the actual evaluation of $\mathbf{A}_m(\cdot)$. Otherwise, matrix \mathbf{A}_m is refreshed in the actual approximation $\xi_{\ell-1}^m$. In our experience, this strategy slightly increases the number of iterations ℓ to satisfy the stopping criterion but it saves the computational time since evaluation of the right-hand side $\mathbf{f}_m(\xi_{\ell-1}^m)$ is much cheaper than the evaluation of $\mathbf{A}_m(\xi_{\ell-1}^m)$, and the factorization of the preconditioner (cf. Section 4) is also kept.

At each step ℓ of the nonlinear iterative solver (17b), we have to solve the linear algebraic system which is discussed in Section 4.

3.5. Stopping criteria for iterative solver and choice of the time steps

Finally, we briefly mention the remaining parts of the computational process, particularly, the choice of the time steps $\tau_m = |I_m|$, $m = 1, \dots, r$ in (10) and (13), and the stopping criteria for nonlinear iterative process (17). Obviously,

the errors arising from the space and time discretization have to be balanced, and the algebraic errors should be below the discretization one.

Therefore, in virtue of [14, 17], for each time level $m = 1, \dots, r$, we define the estimators

$$\eta_m^A(w_{h\tau}) := \sup_{0 \neq \psi_h \in S_m^{h,\tau}} \frac{A_{h,m}(w_{h\tau}, \psi_h)}{\|\psi_h\|_X}, \quad \eta_m^S(w_{h\tau}) = \sup_{0 \neq \psi_h \in S_m^{h,\tau}} \frac{A_{h,m}(w_{h\tau}, \psi_h)}{\|\psi_h\|_X}, \quad \eta_m^T(w_{h\tau}) = \sup_{0 \neq \psi_h \in S_m^{h,\tau+}} \frac{A_{h,m}(w_{h\tau}, \psi_h)}{\|\psi_h\|_X}, \quad (19)$$

where $S_m^{h,\tau}$ is given by (6) and

$$\begin{aligned} S_m^{h,\tau} &:= \left\{ \psi : \Omega \times I_m \rightarrow \mathbb{R}^n; \quad \psi(x, t)|_{K \times I_m} = \sum_{j=0}^q t^j \varphi(x), \quad \varphi \in [P_{p_K+1}(K)]^n, \quad K \in \mathcal{T}_{h,m} \right\}, \\ S_m^{h,\tau+} &:= \left\{ \psi : \Omega \times I_m \rightarrow \mathbb{R}^n; \quad \psi(x, t)|_{K \times I_m} = \sum_{j=0}^{q+1} t^j \varphi(x), \quad \varphi \in [P_{p_K}(K)]^n, \quad K \in \mathcal{T}_{h,m} \right\}, \end{aligned} \quad (20)$$

are its enrichment with respect to space and time. In addition, $\|\psi\|_X = (\|\psi\|_{L^2(\Omega \times I_m)}^2 + \|\nabla \psi\|_{L^2(\Omega \times I_m)}^2 + \|\partial_t \psi\|_{L^2(\Omega \times I_m)}^2)^{1/2}$. We showed in [17] that η_m^S and η_m^T correspond to the spatial and temporal discretization errors and η_m^A corresponds to the algebraic error. Obviously, $\eta_m^A(w_{h\tau}) = 0$ for the exactly computed solution $w_{h\tau}$ of (15). Hence, we stop the nonlinear iterative process (17) if the following condition is valid

$$\eta_m^A(w_{h\tau}) \leq C_A \min(\eta_m^S(w_{h\tau}), \eta_m^T(w_{h\tau})), \quad \text{where } C_A \in (0, 1). \quad (21)$$

Similarly, the time step τ_m is chosen such that

$$\eta_m^T(w_{h\tau}) \approx C_T \eta_m^S(w_{h\tau}), \quad \text{where } C_T \in (0, 1). \quad (22)$$

For more details, we refer to [14, 17].

3.6. Anisotropic mesh adaptation

We briefly mention the main idea of the *anisotropic hp-mesh adaptation method* (*hp*-AMA) developed in [14, 18]. The idea is to define a sequence of meshes $\mathcal{T}_{h,m}$ and spaces $S_m^{h,\tau}$ for all $m = 1, \dots, r$ such that the interpolation error is under the given tolerance, and $N_m = \dim S_m^{h,\tau}$ is minimal. The interpolation error is estimated from a higher-order local reconstruction of the quantity of interest (typically the density) by a least square method where the available information from neighboring elements is employed. If the interpolation error estimate is below the tolerance, we use the given mesh for the next time step, otherwise a re-meshing is carried out and the time step has to be repeated.

The re-meshing techniques construct the new mesh and piecewise polynomial space by minimizing N_m . The anisotropic *hp*-mesh adaptation technique admits to modify size, shape and orientation of mesh elements, as well as local polynomial approximation degree with respect to space. The resulting meshes are non-matching, non-nested but the solution on consequent time intervals are joined together by the time penalty, cf. Section 3.3. For details, we refer to [16].

4. Domain decomposition preconditioners

Now, we focus on the solution of the sequence of linear algebraic systems (17b) which are solved iteratively by the GMRES method with domain decomposition based preconditioners. Therefore, instead of $\mathbf{A}_m \mathbf{d} = \mathbf{f}_m$, we solve the preconditioned system $\mathbf{N}_m^{-1} \mathbf{A}_m \mathbf{d} = \mathbf{N}_m^{-1} \mathbf{f}_m$, where $\mathbf{N}_m^{-1} \approx \mathbf{A}_m^{-1}$, and the applications of \mathbf{N}_m^{-1} can be carried out cheaply. We employ *two-level additive* and/or *hybrid Schwarz* techniques [45, Chapter 2], whose application in the context of discontinuous Galerkin discretization is very straightforward and efficient.

4.1. Domain partition

Let Ω_m^i be open subdomains forming a non-overlapping domain decomposition of the computational domain Ω at time level $i = 1, \dots, m$ such that $\Omega_m^i \cap \Omega_m^j = \emptyset$ for $i \neq j$, and $\bar{\Omega} = \cup_{i=1, \dots, M_m} \bar{\Omega}_m^i$. The subdomains Ω_m^i are defined as a union of some (typically adjacent) elements $K \in \mathcal{T}_{h,m}$. An approach to define Ω_m^i , $i = 1, \dots, M_m$ is to employ

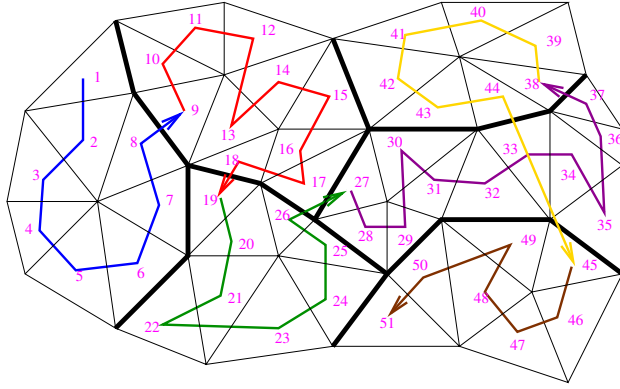


Figure 1: Example of the numbering of mesh elements, bold lines correspond to the boundaries among subdomains Ω_m^i , $i = 1, \dots, M_m$.



Figure 2: Example of a triangulation $\mathcal{T}_{h,m}$ and the block structures of the corresponding matrix \mathbf{A}_m . Left: triangles with polynomial approximation degrees and the domain partition into four subdomains (blue lines). Center: element blocks of \mathbf{A}_m (small red boxes) and the subdomain-blocks \mathbf{A}_i^i , $i = 1, \dots, 4$ (large blue boxes). Right: domain decomposition having four subdomains (colored) and the coarse grid $\mathcal{T}_{h,m}$ with 16 coarse elements (thick lines).

graph partitioning software, e.g., METIS [28], the corresponding sub-meshes are denoted as $\mathcal{T}_{h,m}^i$, $i = 1, \dots, M_m$. We assume that the basis functions from $\mathcal{B}_{h,m}$ (cf. (7)) are numbered so that first we number the test functions with support in Ω_m^1 , then the functions with support in Ω_m^2 , etc. The numbering is illustrated in Figure 1.

In virtue of this numbering, the matrix \mathbf{A}_m from (16) has a natural subdomain-block structure. Figure 2 (left and center) shows an example of a triangulation and the subdomain-block structure of the corresponding matrix \mathbf{A}_m . The left figure shows a mesh with polynomial approximation degrees and the domain partition into four subdomains Ω_m^i , $i = 1, \dots, 4$. The central figure shows the block structure of matrix \mathbf{A}_m (small red boxes). At each block row, there is a square diagonal element-block and up to 3 off-diagonal element-blocks corresponding to a pair of neighboring triangles. These blocks are typically full.

Moreover, matrix \mathbf{A}_m consists of subdomain-blocks $\mathbf{A}_m^{i,j}$, $i, j = 1, \dots, M_m$, which correspond to terms (cf. (16))

$$\mathbf{A}_m^{i,j} : A_{h,m}^L(\cdot, \psi_\beta, \psi_\alpha), \quad K_\alpha \subset \Omega_m^i, \quad K_\beta \subset \Omega_m^j, \quad (23)$$

where K_α and K_β are elements defining multi-indices α and β , respectively, cf. Section 3.1. Obviously, $\mathbf{A}_m^{i,j}$ are vanishing if Ω_m^i and Ω_m^j do not have a common boundary including the case when Ω_m^i and Ω_m^j touch only in one point. Additionally, the diagonal subdomain-blocks $\mathbf{A}_m^{i,i}$ correspond to elements from the same subdomain Ω_m^i , $i = 1, \dots, M_m$,

cf. Figure 2 (center). To shorten the notation, we set $\mathbf{A}_m^i := \mathbf{A}_m^{i,i}$, $i = 1, \dots, M_m$.

The space $S_m^{h,\tau}$ (cf. (6)) is naturally decomposed into local spaces on $\Omega_m^i \times I_m$,

$$S_{m,i}^{h,\tau} := \left\{ \psi : \Omega_m^i \times I_m \rightarrow \mathbb{R}^n; \psi = \varphi|_{\Omega_m^i \times (0,T)}, \varphi \in S_m^{h,\tau} \right\}, \quad i = 1, \dots, M_m, \quad m = 0, \dots, r. \quad (24)$$

We denote $N_m^i = \dim S_{m,i}^{h,\tau}$. Let $\mathbf{R}_{m,i} \in \mathbb{R}^{N_m^i \times N_m^i}$, $i = 1, \dots, M_m$, be the matrix representation of the restriction operator from $S_m^{h,\tau}$ to $S_{m,i}^{h,\tau}$ by the identity on Ω_m^i and by zero on Ω_m^j , $j \neq i$. Denoting $\mathbf{R}_{m,i}^\top$ the transposed operator of $\mathbf{R}_{m,i}$, the diagonal subdomain-blocks fulfil

$$\mathbf{A}_m^i = \mathbf{R}_{m,i} \mathbf{A}_m \mathbf{R}_{m,i}^\top, \quad i = 1, \dots, M_m. \quad (25)$$

4.2. Coarse subspace

To accelerate the transmission of information among subdomains, a two-level method is employed. Therefore, for each $m = 1, \dots, r$, we consider a coarse mesh $\mathcal{T}_{H,m} = \{\mathcal{K}\}$, which consists of polygonal elements \mathcal{K} . We define $\mathcal{K} \in \mathcal{T}_{H,m}$ by dividing every subdomain Ω_m^i to several “sub-subdomains”, each of them forming one element \mathcal{K} , see Figure 2 (right). Then any $\mathcal{K} \in \mathcal{T}_{H,m}$ belongs to only one subdomain Ω_m^i including the case $\mathcal{K} = \overline{\Omega}_i$ for some $i = 1, \dots, M_m$. In this paper, we restrict to the case when each subdomain Ω_m^i , $i = 1, \dots, M_m$, is split into a constant number of s_m coarse elements, $s_m \in \mathbb{N}$. Hence, the coarse mesh has $\#\mathcal{T}_{H,m} = s_m M_m$ elements for all $m = 1, \dots, r$.

Let $p_{\mathcal{K}} = \min_{K \subset \mathcal{K}} p_K$, $d_{\mathcal{K}} := (p_{\mathcal{K}} + 1)(p_{\mathcal{K}} + 2)/2$ for $\mathcal{K} \in \mathcal{T}_{H,m}$, we define the coarse finite element spaces

$$S_m^{H,\tau} := \left\{ \psi : \Omega \times I_m \rightarrow \mathbb{R}^n; \psi(x, t)|_{\mathcal{K} \times I_m} = \sum_{j=0}^q t^j \phi(x), \phi \in [P_{p_{\mathcal{K}}}(\mathcal{K})]^n, \mathcal{K} \in \mathcal{T}_{H,m} \right\}, \quad m = 0, \dots, r, \quad (26)$$

cf. (6). Similarly as in (7), we define the basis $\mathcal{B}_{H,m}$ of spaces $S_m^{H,\tau}$ by replacing the symbol K by \mathcal{K} and h by H , i.e.,

$$\mathcal{B}_{H,m} := \left\{ \psi_{\alpha}, \psi_{\alpha} := \psi_{\mathcal{K},k,i}^j, \alpha = \{\mathcal{K}, k, i, j\} \quad \forall \alpha \in B_{H,m} \right\}, \quad (27)$$

where $B_{H,m}$ is the set of all multi-indices $\alpha = \{\mathcal{K}, k, i, j\} : j = 0, \dots, q, i = 1, \dots, d_{\mathcal{K}}, k = 1, \dots, n, \mathcal{K} \in \mathcal{T}_{H,m}$.

Obviously, $S_m^{H,\tau} \subset S_m^{h,\tau}$ for all $m = 1, \dots, r$. Therefore, any basis function from $\mathcal{B}_{H,m}$, can be expressed as a linear combination of basis function from $\mathcal{B}_{h,m}$, cf. (7). The coefficients of these linear combinations defines the *restriction matrix* $\mathbf{R}_0 \in \mathbb{R}^{N_m^0 \times N_m}$ where N_m^0 is the dimension of $S_m^{H,\tau}$ given analogously as (14). Let \mathbf{R}_0^\top be its transpose representing the prolongation operator. Then we set the coarse matrix

$$\mathbf{A}_m^0 := \mathbf{R}_0 \mathbf{A}_m \mathbf{R}_0^\top \in \mathbb{R}^{N_m^0 \times N_m^0}, \quad m = 1, \dots, r. \quad (28)$$

Remark 4.1. In virtue of (16) and the definition of \mathbf{R}_0 , the matrix \mathbf{A}_m^0 from (28) fulfils

$$\mathbf{A}_m^0(\tilde{\xi}) = \left\{ (\mathbf{A}_m^0(\tilde{\xi}))_{\alpha\beta} \right\}_{\alpha, \beta \in B_{H,m}}, \quad (\mathbf{A}_m^0(\tilde{\xi}))_{\alpha\beta} = A_{h,m}^1(\tilde{w}, \psi_{\beta}, \psi_{\alpha}), \quad \alpha, \beta \in B_{H,m}. \quad (29)$$

Hence, \mathbf{A}_m^0 can be evaluated directly from (10) inserting the basis function from $\mathcal{B}_{H,m}$ to the second and third arguments of $A_{h,m}^1$. Although both (28) and (29) are equivalent, the approach (29) is less robust in the finite precision arithmetic when solving the Navier-Stokes equations. On the other hand, we have not observed this effect for scalar problems ($n = 1$ in (1)).

4.3. Additive and hybrid preconditioners

We introduce the additive and hybrid two-level Schwarz preconditioners which are suitable for parallelization. We present only the final formulas, for details we refer, e.g., to [45, Chapter 2]. The *additive preconditioned operator* is additive in the local problems as well as the global coarse one, and it reads

$$\mathbf{P}_{\text{add},2} := \sum_{i=0}^{M_m} \mathbf{P}_{m,i}, \quad \text{where} \quad \mathbf{P}_{m,i} := \mathbf{R}_{m,i}^\top (\mathbf{A}_m^i)^{-1} \mathbf{R}_{m,i} \mathbf{A}_m, \quad i = 0, \dots, M_m. \quad (30)$$

Algorithm 1: Application of the preconditioner $\mathbf{N}_{\text{add},2}^{-1}$ from (31): $\mathbf{u} \leftarrow \mathbf{N}_{\text{add},2}^{-1} \mathbf{x}$

- 1: **input** matrices $\mathbf{A}_m, \mathbf{A}_m^i, \mathbf{R}_{m,i}, i = 0, \dots, N$, vector \mathbf{x}
- 2: set $\mathbf{x}_i := \mathbf{R}_{m,i} \mathbf{x}$ and solve $\mathbf{A}_m^i \mathbf{y}_i = \mathbf{x}_i$ for $i = 0, \dots, N$
- 3: **output** vector $\mathbf{u} := \sum_{i=0}^N \mathbf{R}_{m,i}^T \mathbf{y}_i$

Algorithm 2: Application of the preconditioner $\mathbf{N}_{\text{hyb}}^{-1}$ from (33): $\mathbf{u} \leftarrow \mathbf{N}_{\text{hyb}}^{-1} \mathbf{x}$

- 1: **input** matrices $\mathbf{A}_m, \mathbf{A}_m^i, \mathbf{R}_{m,i}, i = 0, \dots, N$, vector \mathbf{x}
- 2: set $\mathbf{x}_i := \mathbf{R}_{m,i} \mathbf{x}$ and solve $\mathbf{A}_m^i \mathbf{y}_i = \mathbf{x}_i$ for $i = 1, \dots, N$
- 3: $\mathbf{y} := \sum_{i=1}^N \mathbf{R}_{m,i}^T \mathbf{y}_i$
- 4: $\mathbf{z} := \mathbf{x} - \mathbf{A}_m \mathbf{y}$
- 5: $\mathbf{x}_0 := \mathbf{R}_0 \mathbf{z}$ and solve $\mathbf{A}_m^0 \mathbf{y}_0 = \mathbf{x}_0$
- 6: **output** vector $\mathbf{u} := \mathbf{R}_0^T \mathbf{y}_0 + \mathbf{y}$

Since $\mathbf{P}_{\text{add},2} = \mathbf{N}_{\text{add},2}^{-1} \mathbf{A}_m$, the corresponding preconditioner has the form

$$\mathbf{N}_{\text{add},2}^{-1} = \sum_{i=0}^{M_m} \mathbf{R}_{m,i}^T (\mathbf{A}_m^i)^{-1} \mathbf{R}_{m,i}. \quad (31)$$

On the other hand, the hybrid preconditioner is additive in the local components but multiplicative with respect to the levels. The *hybrid preconditioned operator* reads

$$\mathbf{P}_{\text{hyb}} := \mathbf{I} - (\mathbf{I} - \mathbf{P}_0)(\mathbf{I} - \sum_{i=1}^N \mathbf{P}_{m,i}), \quad (32)$$

where $\mathbf{P}_{m,i}$ are given in (30). Since $\mathbf{P}_{\text{hyb}} := \mathbf{N}_{\text{hyb}}^{-1} \mathbf{A}_m$, the hybrid preconditioner can be written in the form

$$\mathbf{N}_{\text{hyb}}^{-1} = \sum_{i=1}^N \mathbf{R}_{m,i}^T (\mathbf{A}_m^i)^{-1} \mathbf{R}_{m,i} + \mathbf{R}_0^T (\mathbf{A}_m^0)^{-1} \mathbf{R}_0 \left(\mathbf{I} - \mathbf{A}_m \sum_{i=1}^N \mathbf{R}_{m,i}^T (\mathbf{A}_m^i)^{-1} \mathbf{R}_{m,i} \right). \quad (33)$$

We note that the hybrid preconditioned operator (32) is not symmetric. Therefore, a modification for symmetric problems is required. However, the systems treated in our paper are not symmetric so the form (32) is applicable.

Algorithms 1 and 2 describe the applications of preconditioners $\mathbf{N}_{\text{add},2}^{-1}$ and $\mathbf{N}_{\text{hyb}}^{-1}$ introduced in (31) and (33). While Algorithm 1 allows to solve the local fine problems (with $\mathbf{A}_m^i, i = 1, \dots, N$) together with the global coarse problem (with \mathbf{A}_m^0) in parallel, Algorithm 2 requires solving the local fine problems first and then solving the global coarse problem. Additionally, one multiplication by \mathbf{A}_m has to be performed. The multiplication by \mathbf{A}_m is typically cheaper than the solution of the local or coarse problems. Moreover, if the global coarse problem is smaller than a local one, then the application of the preconditioner $\mathbf{N}_{\text{hyb}}^{-1}$ exhibits only a small increase of the computational time in comparison to the preconditioner $\mathbf{N}_{\text{add},2}^{-1}$. Additionally, the hybrid preconditioner is typically more efficient, and a smaller number of GMRES iterations has to be carried out to achieve the given tolerance.

The application of the two-level preconditioners in Algorithms 1 and 2 exhibits the solution of the local (fine) systems and the global (coarse) one,

$$\mathbf{A}_m^i \mathbf{y}_i = \mathbf{x}_i, \quad i = 1, \dots, M_m, \quad \text{and} \quad \mathbf{A}_m^0 \mathbf{y}_0 = \mathbf{x}_0, \quad \text{respectively.} \quad (34)$$

We solve these systems directly by the MUMPS library [3, 4, 34], which consists of two steps:

(Sa) the *factorization* of the system, which is carried out after the evaluation of \mathbf{A}_m ,

(Sb) the *substitution* of the solution which is carried out in each GMRES iteration.

We note that the term “substitution” means the evaluation of the solution using the factorization of the matrix and

it is called “assembling” in MUMPS. However, in the finite element community, the assembling usually means the creation of the matrix itself, so we use the term substitution.

4.4. Problem formulation

The numerical method described in Section 3 requires the solution of a sequence of linear algebraic systems

$$\mathbf{A}_m(\xi_{\ell-1}^m) \mathbf{d}_\ell = \mathbf{f}_m(\xi_{\ell-1}^m), \quad \ell = 1, 2, \dots, \quad m = 1, \dots, r, \quad (35)$$

where ℓ denotes the Newton iterates and m the time level, cf. (17b). We solve (35) by GMRES with two-level preconditioners described in Section 4.3. Finally, the GMRES solver is stopped when the norm of the preconditioned residual decreases by a fixed factor $C_I \ll 1$. Hence, the algebraic error is controlled by (21) only.

These preconditioners have to solve M_m local problems defined on subdomains Ω_m^i , $i = 1, \dots, M_m$, and the global problem on a coarse mesh having $\#\mathcal{T}_{H,m} = s_m M_m$ elements, where $s_m \geq 1$ is a chosen integer. We recall that we consider the case when each Ω_m^i , $i = 1, \dots, M_m$, is divided into s_m coarse elements. The fundamental question studied in this paper is the following.

Problem 4.2. Let $S_m^{h,\tau}$, $m = 1, \dots, r$ be, the sequence of finite element spaces (6) generated by hp -AMA (cf. Section 3.6) used for the solution of (1) by STDGM (cf. Section 3). How to choose M_m and s_m , $m = 1, \dots, r$, such that the solution of the arising sequence of linear systems (35) by GMRES with two-level preconditioners requires the shortest possible wall-clock time in a parallel computation?

Obviously, larger M_m admits to use more computer cores, but the GMRES solver requires more iterations. On the other hand, a fine coarse mesh $\mathcal{T}_{H,m}$ increases the speed of convergence, but the corresponding coarse problem is more expensive to solve. Moreover, the real wall-clock time depends on many factors. Apart of the numerical scheme itself, also on its implementation, the speed of communication among the cores of the computer, their type, etc. Therefore, we introduce a simplified computational cost model which takes into account the number of floating point operations, the speed of computation (performance), and the wall-clock time of the communication among the cores of the computer.

5. Computational costs

In this section, we introduce the simplified model which will measure the computational costs of the preconditioners which exhibits the most time-consuming part of the whole process. Based on this model, we propose an adaptive algorithm giving an approximation of Problem 4.2.

5.1. Quantities defining the computational costs

To define the computational cost model, we introduce the following assumptions.

- (A1) The applications of the two-level preconditioner, i.e., the solution of systems (34), is the dominant part of the computational process. The other parts, such as the evaluation of entries of matrix \mathbf{A}_m in (16) and vector \mathbf{f}_m in (15), multiplication of a vector by matrix \mathbf{A}_m in GMRES, the computational overheads, etc., can be neglected.
- (A2) Enough computer cores are available such that each local system in (34) can be solved in parallel, and also each \mathbf{A}_m^i , $i = 0, \dots, M_m$ is stored only at a separate core. Therefore, the factorization of the local systems and the global coarse one can be carried out simultaneously in parallel.
- (A3) All vectors appearing in the computations are stored in copies at each used computer core. Therefore, in virtue of the previous item, the communication among the cores is represented just by the output of (34) sent from each core and received by every core.
- (A4) Only the following communications among the cores are considered:
 - (a) The solution of the local systems (34) for $i = 1, \dots, M_m$ gives the local vectors \mathbf{y}_i which have to be joined together and spread among all cores. We denote this communication *allgather* and use the subroutine *MPI_Allgatherv* in MPI [33].

(b) The solution of the coarse system (34) for $i = 0$ gives the local vector \mathbf{y}_0 which has to be spread among all cores. We denote this communication *bcast* and use the subroutine *MPI_Bcast* in MPI [33].

We are aware that the previous assumptions exhibit a strong simplification, yet they allow us to define a relatively simple computational cost model which can provide useful information. The previous assumptions can be relaxed by incorporating the corresponding items in a more complex model.

Remark 5.1. It is possible to consider an alternative implementation, in which the coarse problem is stored in copies at each core. Then *bcast* can be avoided but the coarse problem can not be factorized simultaneously with the local ones. Consequently, the subsequent computational model would have to be modified.

The goal of the computational cost model is not only to measure the computational costs but also to predict them for a priori unknown domain decomposition. Therefore, we consider

- (T1) the number of *floating point operations (flops)* per each task of the algorithm and each core,
- (T2) the *speed of the computations* (= performance) per each task of the algorithm and each core,
- (T3) the wall-clock time of *communication operations* among the cores.

We note that the number of *flops* necessary to solve (34) are provided by the MUMPS library, cf. Section 5.3.1.

5.2. Simplified model of the algorithm on parallel computer

For the setting of the computational costs, we use an algorithm implementation sketched in Figure 3. The algorithm is split into several task levels $J = 1, 2, \dots$, and each task level is split into M tasks, one task for one core I , $I = 1, \dots, M$. The performance of each task on each core is independent of the performance of other tasks and cores. We denote by T_J^I the task on task level $J = 1, 2, \dots$ and the core $I = 1, \dots, M$. When all tasks T_J^I , $I = 1, \dots, M$ from one task level J are finished, the cores are synchronized, the particular outputs are transmitted among the cores, and we proceed to the next task level $J + 1$. Let wt_J^I denote the wall-clock time to carry out task T_J^I , $I = 1, \dots, M$, $J = 1, 2, \dots$, then we define the wall-clock time for task level J by

$$\text{wt}_J := \max_{I=1, \dots, M} \text{wt}_J^I, \quad J = 1, 2, \dots \quad (36)$$

By ct_J we denote the wall-clock time necessary to transmit data from level J to level $J + 1$. Consequently the total wall-clock time of the algorithm is given by

$$\text{wt} := \sum_{J=1,2,\dots} (\text{wt}_J + \text{ct}_J). \quad (37)$$

Note that the measure wt_J can be seen as the wall-clock time needed by one core with the largest amount of work (longest time) at level J . In the following, we study the particular task levels of the algorithm in terms of (T1)–(T3) under Assumptions (A1)–(A4). Therefore, we consider only the factorization and substitution of the local and coarse global systems (34).

5.3. Computational cost model

First, we introduce the following notation which relates to the discretization and the computational process introduced in Sections 3 and 4. Let $m = 1, \dots, r$ be arbitrary but fixed index of the time layer.

- $\#\mathcal{T}_{h,m}$ – number of elements of mesh $\mathcal{T}_{h,m}$,
- N_m ($= \dim S_m^{h,\tau}$) – the size of matrix \mathbf{A}_m ,
- M_m – the number of subdomains of domain decomposition,
- s_m – the number of coarse elements in each subdomain, the number of coarse elements is $\#\mathcal{T}_{H,m} = s_m M_m$,
- it_m^n – the number of Newton (nonlinear) iterations in time step m ,
- it_m^ℓ – the number of GMRES (linear) iterations over all nonlinear iterations it_m^n in time step m ,
- \mathcal{F}_m^A – the number of evaluations of matrix \mathbf{A}_m from (16) in time step m .

We note that $\mathcal{F}_m^A \leq \text{it}_m^n$ and the equality is valid if the matrix \mathbf{A}_m is updated at each Newton iteration. However, in virtue of Remark 3.2, the value \mathcal{F}_m^A is smaller in practice. In the following paragraphs, we discuss the particular part of the computation in terms (T1)–(T3) in one time step m .

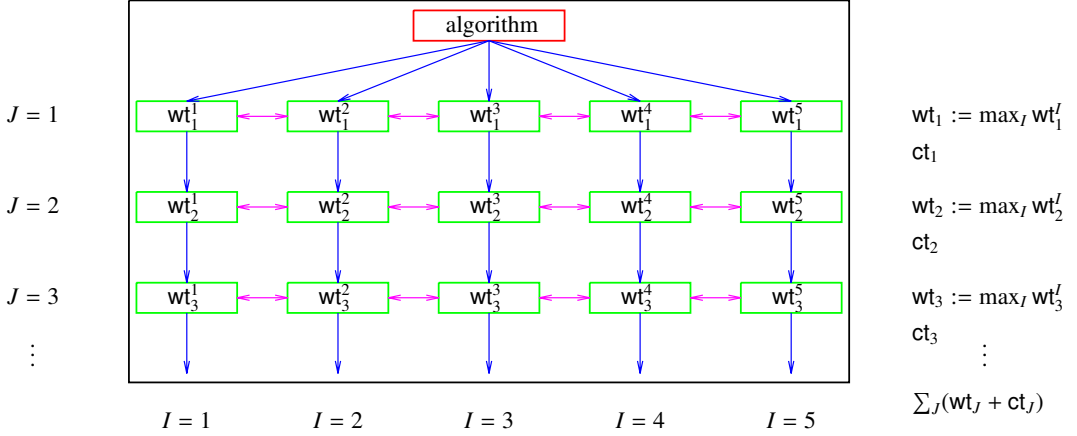


Figure 3: Computational cost model using 5 cores $I = 1, \dots, 5$, parallel computations (green boxes) followed by communication among cores (magenta arrows), and subsequent steps of the algorithm (blue arrows).

5.3.1. Floating point operations

The solution of systems (34) by MUMPS consists of the factorization of the matrices (step (Sa)) and the substitution of the solution (step (Sb)). While step (Sa) is performed only after the refreshing of \mathbf{A}_m (i.e., F_m^A times), the substitution is carried out at each GMRES iterations.

Let $\text{flops}_{\text{fac}}^{m,i}$ and $\text{flops}_{\text{sub}}^{m,i}$ denote the number of floating point operations for factorization of \mathbf{A}_m^i and substitution of the corresponding solutions, respectively, $i = 0, \dots, M_m$. The factorization of \mathbf{A}_m^i can be carried out independently for each $i = 0, \dots, M_m$, so in virtue of (36), the maximum of the number of floating point operations per core is

$$\text{flops}_{\text{fac}}^m := \max_{i=0, \dots, M_m} \text{flops}_{\text{fac}}^{m,i}. \quad (38)$$

Note that index 0 is included and stands for the coarse problem. On the other hand, the substitution of the solutions of the local systems and the global coarse one (34) is executed in parallel only for the additive preconditioner $\mathbf{N}_{\text{add},2}^{-1}$ (31). For the hybrid preconditioner $\mathbf{N}_{\text{hyb}}^{-1}$ (33), we solve the local systems in parallel and then the global system sequentially. Hence, the corresponding maximum of the number of floating point operations per core for substitution is

$$\text{flops}_{\text{sub}}^m := \begin{cases} \max_{i=0, \dots, M_m} \text{flops}_{\text{sub}}^{m,i} & \text{for } \mathbf{N}_{\text{add},2}^{-1}, \\ \max_{i=1, \dots, M_m} \text{flops}_{\text{sub}}^{m,i} + \text{flops}_{\text{sub}}^{m,0} & \text{for } \mathbf{N}_{\text{hyb}}^{-1}, \end{cases} \quad (39)$$

in each GMRES iteration. Therefore, in virtue of (36)–(37), the total number of flops per one node is given by

$$\text{flops}^m = \mathsf{F}_m^A \text{flops}_{\text{fac}}^m + \text{it}_m^\ell \text{flops}_{\text{sub}}^m, \quad m = 1, \dots, r. \quad (40)$$

We note that the substitution at each time step is carried out $\text{it}_m^\ell + \text{it}_m^n$ times since the preconditioner has to be applied also to the right-hand side of (35) in each Newton iterate. However, the value it_m^ℓ is typically several times larger than it_m^n , hence the latter can be omitted in (40).

To establish the computational cost model, we are interested in the dependence of $\text{flops}_{\text{fac}}^{m,i}$ and $\text{flops}_{\text{sub}}^{m,i}$ on the size of the systems N_m^i , $i = 0, \dots, M_m$. These values depend on the sparsity and shape of the matrices \mathbf{A}_m^i and therefore on meshes $\mathcal{T}_{h,m}$, $\mathcal{T}_{H,m}$, polynomial degrees, etc. We carried out a series of numerical experiments when the Navier-Stokes equations (1) were discretized by STDG method (13) on several quasi-uniform meshes $\mathcal{T}_{h,m}$ and coarse meshes $\mathcal{T}_{H,m}$ with fixed temporal degree $q = 1$ and uniform spatial degrees $p_K = 1, \dots, 6$, $K \in \mathcal{T}_{h,m}$. The resulting algebraic systems \mathbf{A}_m and \mathbf{A}_m^0 were factorized and substituted by MUMPS (cf. (Sa)–(Sb)) which provides the corresponding number of flops (variables `mumps_par%RINFOG(1:2)` in [34, User's guide]). We consider the coarse meshes $\mathcal{T}_{H,m}$ separately since they are polygonal and their sparsity differs from the sparsity (fine or local) meshes of triangular

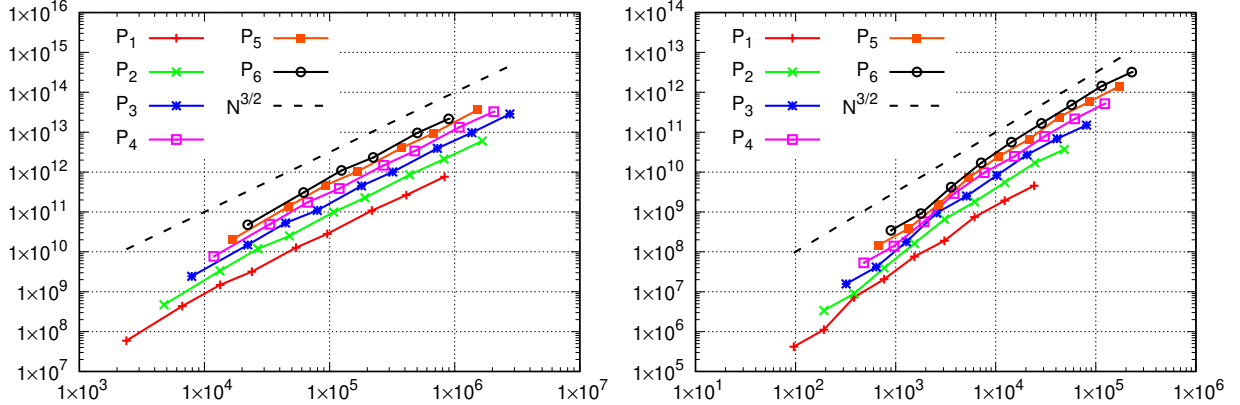


Figure 4: Number of the floating point operations for the matrix factorization: dependence of $\text{flops}_{\text{fac}}^{m,i}$ on the system size N_m^i corresponding to triangular $\mathcal{T}_{h,m}^i$ (left) and polygonal $\mathcal{T}_{H,m}$ (right) grids.

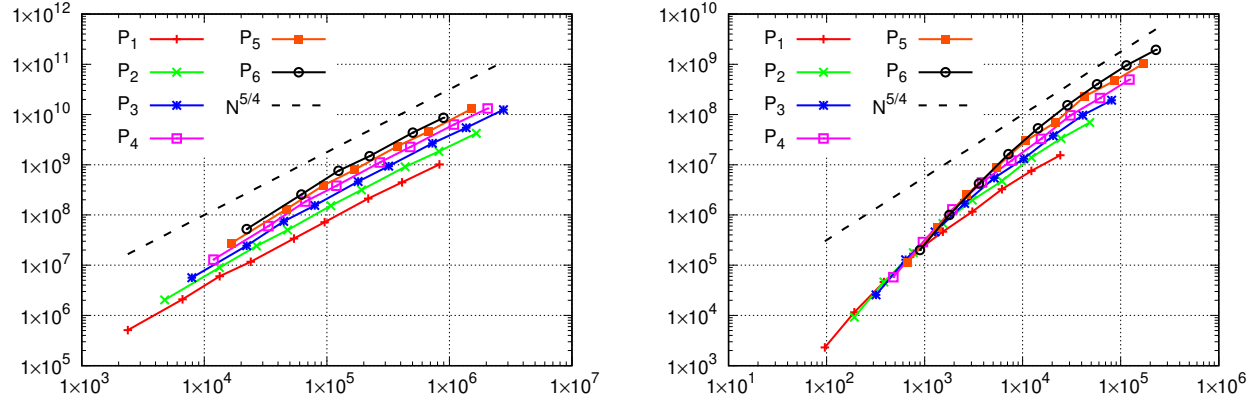


Figure 5: Number of the floating point operations for the solution substitution: dependence of $\text{flops}_{\text{sub}}^{m,i}$ on the system size N_m^i corresponding to triangular $\mathcal{T}_{h,m}^i$ (left) and $\mathcal{T}_{H,m}$ (right) grids.

elements.

Numerical results are given in Figures 4 and 5, they show the dependence of the values $\text{flops}_{\text{fac}}^{m,i}$ and $\text{flops}_{\text{sub}}^{m,i}$ on the system size, respectively, in logarithmic scale. We easily deduce an asymptotic exponential dependence

$$\text{flops}_{\text{fac}}^{m,i}(N) \approx C N^\mu, \quad \text{flops}_{\text{sub}}^{m,i}(N) \approx c N^\nu, \quad i = 1, \dots, M_m, \quad (41)$$

where c , C , μ and ν are positive parameters. More detailed inspection indicates the values $\mu \approx 3/2$ and $\nu \approx 5/4$ for all polynomial degrees p whereas the constants c and C are p -dependent. It is caused by the increasing sparsity of matrices for increasing p . The empirical formulas (41) are used later for the prediction of the number of floating point operations.

5.3.2. Speed of the computation

Although the number of flops discussed in Section 5.3.1 gives reasonable information about the computational costs, it does not fully reflect the wall-clock time which is the desired interest in practical computations. The wall-clock time does not scale linearly with the number of flops typically due to limits to speed of memory access. Therefore, we measure the wall-clock time for the factorization and substitution of the systems in all numerical experiments from Section 5.3.1. We use the function *MPI_Wtime* in the MPI [33] which returns the wall-clock time in seconds (s).

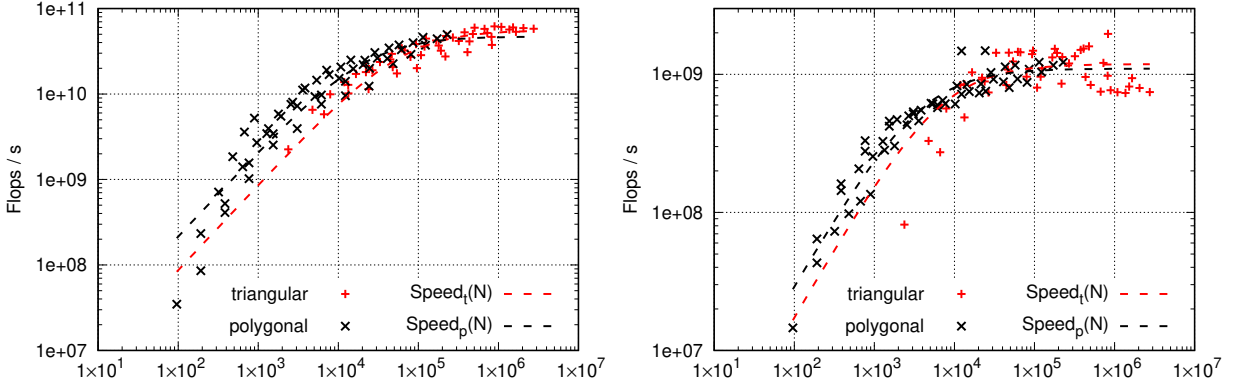


Figure 6: Performance of the matrix factorization and substitution: dependence of $\text{flops}_{\text{fac}}^{m,i} / \text{s}$ (left) and $\text{flops}_{\text{sub}}^{m,i} / \text{s}$ (right) on the system size N_m^i for triangular $\mathcal{T}_{h,m}^i$ (red +) and polygonal $\mathcal{T}_{h,m}$ (black \times). Dashed lines are fitted functions $\text{speed}(N)$ in the form of (43) for both types of meshes and factorization/substitution.

Table 1: Performance of the matrix factorization and substitution, the values of the fitted parameters a and b from (43).

operation	grid	a	b
factorization	triangular	5.5827E+10	6.4325E+04
factorization	polygonal	4.7066E+10	2.1832E+04
substitution	triangular	1.1884E+09	6.7913E+03
substitution	polygonal	1.1009E+09	3.7104E+03

We denote the wall-clock times for the factorization and substitution of (34) by $\text{time}_{\text{fac}}^{m,i}$ and $\text{time}_{\text{sub}}^{m,i}$, $i = 0, \dots, M_m$, respectively. Then the speed of computation of factorization and substitution reads

$$\text{speed}_{\text{fac}}^{m,i} := \frac{\text{flops}_{\text{fac}}^{m,i}}{\text{time}_{\text{fac}}^{m,i}} \quad \text{and} \quad \text{speed}_{\text{sub}}^{m,i} := \frac{\text{flops}_{\text{sub}}^{m,i}}{\text{time}_{\text{sub}}^{m,i}}, \quad i = 0, \dots, M_m, \quad (42)$$

respectively. Figure 6 shows the dependence of $\text{speed}_{\text{fac}}^{m,i}$ and $\text{speed}_{\text{sub}}^{m,i}$ on the size of the system N_m^i in units flops/s . The numerical experiments were carried out using cluster of nodes with 4x Intel Xeon Gold 6240 CPU 2.60GHz, 512GB RAM, interconnected by InfiniBand 100 Gb.

Figure 6 shows that the performance is increasing for increasing size of the system and it is approaching a limit of a maximal performance. Therefore, we estimate a simple empirical dependence

$$\text{speed}(N) \approx \frac{aN}{b + N}, \quad a, b > 0, \quad (43)$$

where a is the maximal speed for $N \rightarrow \infty$. The parameters a and b can be found by fitting the function in the form (43) with the measured data. We have found them iteratively by a nonlinear least square technique, and the corresponding values of a and b from (43) are given in Table 1. The fitted functions are shown also in Figure 6 by dashed lines.

The measuring of the wall-clock time is influenced by several perturbations caused by the system noise, operating system scheduling, etc. These tiny interruptions lead to slight variations in the wall-clock time, up to several percents. Moreover, we observed that the fitting of speed according to formula (43) by the nonlinear least-squares technique is sensitive to data perturbations and initial approximation. Therefore, in practical applications, we replace (43) by an affine approximation, particularly

$$\text{speed}(N) \approx \min(\bar{S}, aN + b), \quad (44)$$

where a and b are the parameters given by a linear least-squares method and \bar{S} is the maximal speed. In practical computation, we set \bar{S} according to formula (53) below. Formula (44) mimics dependence (43) locally, and in our experience, it is less sensitive to data perturbations.

Finally, we recall that from (42), we can estimate time as

$$\text{time}_{\text{fac}}^{m,i} = \frac{\text{flops}_{\text{fac}}^{m,i}}{\text{speed}_{\text{fac}}^{m,i}}, \quad \text{time}_{\text{sub}}^{m,i} = \frac{\text{flops}_{\text{sub}}^{m,i}}{\text{speed}_{\text{sub}}^{m,i}}, \quad i = 0, \dots, M_m, \quad (45)$$

and therefore, using (40) the wall-clock time for the application of the preconditioners for all GMRES iterations within time step m is estimated as

$$\begin{aligned} \text{time}^m &= F_m^A \max_{i=0, \dots, M_m} \text{time}_{\text{fac}}^{m,i} + it_m^\ell \max_{i=0, \dots, M_m} \text{time}_{\text{sub}}^{m,i} & \text{for } N_{\text{add},2}^{-1}, \\ \text{time}^m &= F_m^A \max_{i=0, \dots, M_m} \text{time}_{\text{fac}}^{m,i} + it_m^\ell \left(\max_{i=1, \dots, M_m} \text{time}_{\text{sub}}^{m,i} + \text{time}_{\text{sub}}^{m,0} \right) & \text{for } N_{\text{hyb}}^{-1}. \end{aligned} \quad (46)$$

5.3.3. Communication operations

In virtue of Assumption (A4), we consider only the communications *allgather* and *bcast* which are carried out always after the solution of systems (34), hence once in each GMRES iteration. These communication costs have two fundamental parts: the *latency*, which is the fixed cost of starting a communication, independent of the size of transmitted data, and the *bandwidth* which is the rate at which data can be transferred once the communication has started. According to, e.g., [11, 26], the lower bounds of the latency and bandwidth of *allgather* and *bcast* are given by

$$\text{latency} \approx \alpha \log_2(P), \quad \text{bandwidth} \approx \beta \frac{P-1}{P} N, \quad (47)$$

where P is the number of cores, and N is the length of transmitted data. The parameters α and β are positive constants and they are hardware and software dependent.

To illustrate the dependence of *allgather* and *bcast* on the number of processors P and the size of transmitted data N , we carried out several numerical experiments measuring the wall-clock time of both communications. We denote by $\text{com}_{\text{allgather}}^{m,1}$ and $\text{com}_{\text{bcast}}^{m,1}$ the wall-clock time of *allgather* and *bcast* of one transmission given by Assumption (A4), respectively. To obtain observations close to a real computation, we applied the numerical scheme presented in Sections 3 and 4 for unstructured quasi-uniform meshes \mathcal{T}_h^i , $i = 1, \dots, 4$ having 996, 2248, 3996, and 9074 elements. We considered 80 degrees of freedom per element, hence the size of the corresponding global fine systems was $N = 79\,680, 179\,840, 319\,680$, and $725\,920$. For each mesh, we consider $M = 8, 16, 32$, and 64 subdomains, and each computation was executed with $P = M$ cores. The number of coarse elements was chosen as $2^{i-1} M$ and then the size of small (global coarse) system was $N^0 = 80 \cdot 2^{i-1} M$ for all meshes \mathcal{T}_h^i , $i = 1, \dots, 4$. We note that the size of the local vectors (each local vector is associated to one core) is not the same, hence we use *MPI_Allgatherv* function. The cluster setting and the measurement of the wall-clock time was the same as in Section 5.3.2.

In order to avoid fluctuation in the measurement of the communication time, we carried out at least one thousand of GMRES iterations and present averaged times. The results are given in Figure 7, where we show the dependence of the (averaged) wall-clock time of one *bcast* and one *allgather* communication on the size of transmitted vector (N^0 for *bcast*, N for *allgather*) and on the number of cores P .

We observe the linear dependence $O(N)$ of the wall-clock times for both communications *allgather* and *bcast* on the size of the transmitted vector which is in agreement with the bandwidth (47) (for large P when $(P-1)/P \approx 1$). On the other hand, the dependence of both communications *allgather* and *bcast* on the number of cores is clearly sub-linear but not quite logarithmic. We found empirically the dependence $O(P^{0.7})$, which is depicted in Figure 7 too.

Therefore, in virtue of (47) and the numerical experiments, two variants of the communication cost model are

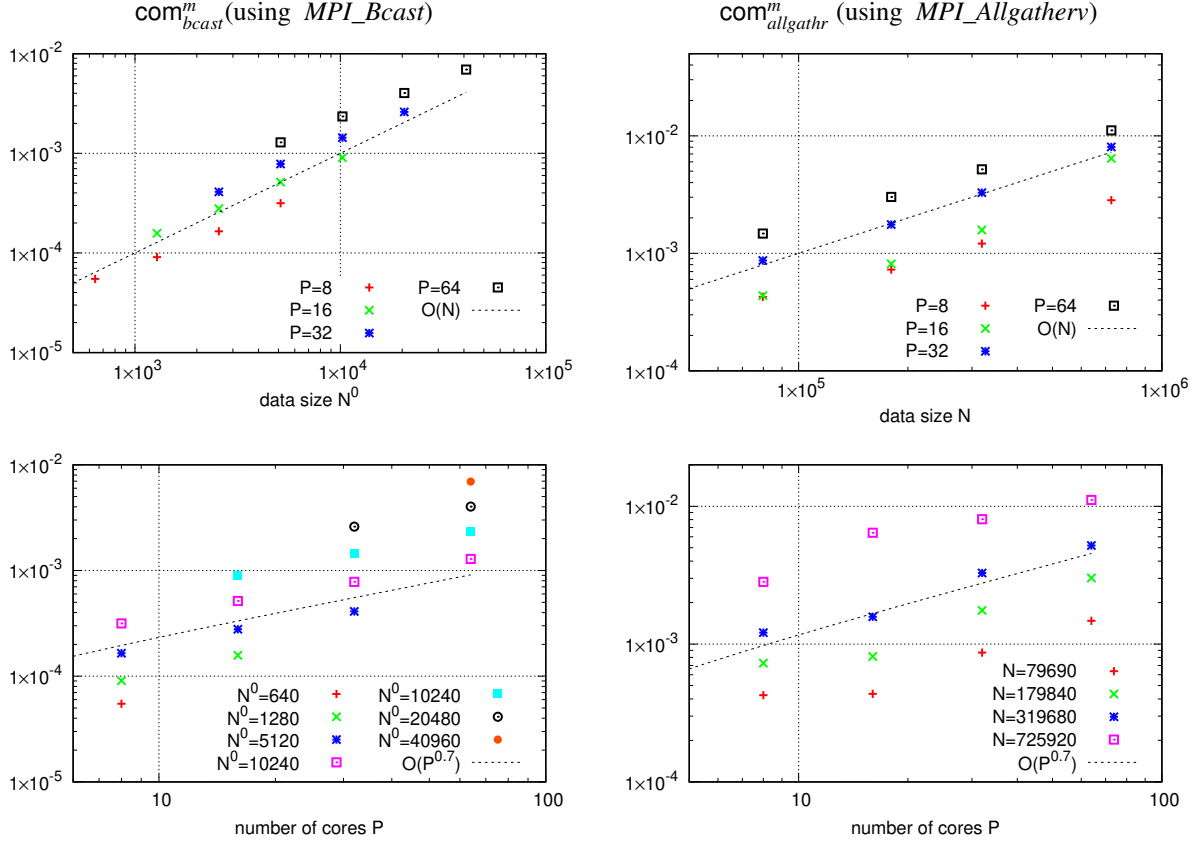


Figure 7: Communication wall-clock time for one *bcast* (left columns) and *allgather* (right columns), the dependence on the size of communicated vectors (top row) and the number of cores (bottom row).

possible:

$$\text{com}_{allgather}^{m,1}(N, P) \approx \alpha_g \log_2 P + \beta_g N + \gamma_g, \quad (48a)$$

$$\text{com}_{allgather}^{m,1}(N, P) \approx \alpha_g (P-1)^{0.7} + \beta_g N + \gamma_g, \quad (48b)$$

where $\text{com}_{allgather}^{m,1}$ and $\text{com}_{bcast}^{m,1}$ are the wall-clock times of *allgather* and *bcast* for one call of *MPI_Allgatherv* and *MPI_Bcast*, respectively. To observe the difference between (48a) and (48b), we found the parameters α_g , β_g , γ_g , α_b , β_b , and γ_b for the data from Figure 7 by the least square technique. The resulting fitted functions are shown in Figure 8, where all data from Figure 7 (blue nodes) are fitted by analytical functions (48a) and (48b). We observe a close approximation of the data. In the following, we use fitting (48a) since it has better theoretical background and may work better also beyond one node.

Finally, we conclude that the communications *bcast* and *allgather* are carried out once in each GMRES iteration, hence the wall-clock time for the communication in m -th time step can be approximated as

$$\text{com}_{allgather}^m(N, P) = \text{it}_m^\ell \text{com}_{allgather}^{m,1}, \quad \text{com}_{bcast}^m(N, P) = \text{it}_m^\ell \text{com}_{bcast}^{m,1}, \quad m = 1, \dots, r. \quad (49)$$

5.4. Final cost model

The summary of considerations from Sections 5.3.1–5.3.3 is to evaluate the computational costs of the numerical method from Sections 3–4 as the sum of the wall-clock times for computation and communications over all time steps

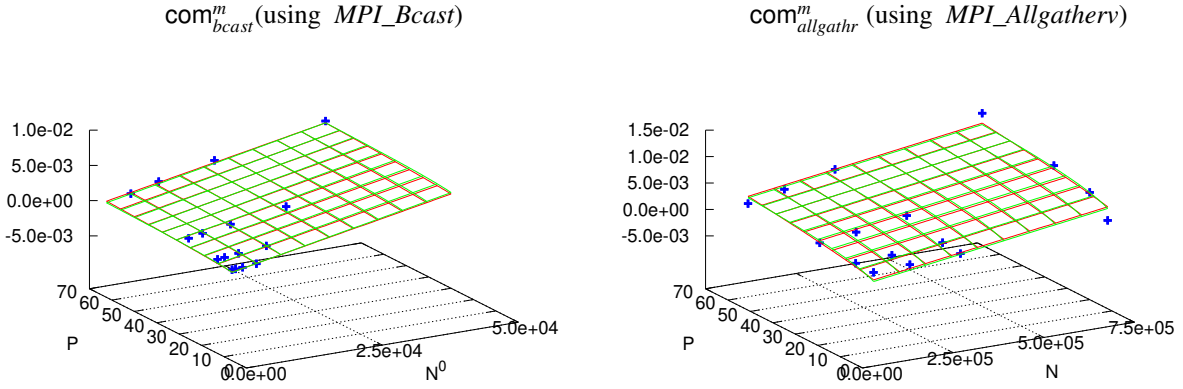


Figure 8: Communication wall-clock time for one *bcast* (left columns) and *allgather* (right columns), the dependence on the size of communicated vectors N and the number of cores P (blue nodes), fitted function using (48a) (green) and (48b) (red).

$m = 1, \dots, r$ as

$$\text{costs} := \sum_{m=1}^r \text{costs}^m, \quad \text{costs}^m := (\text{time}^m + \text{com}^m), \quad m = 1, \dots, r, \quad (50)$$

where $\text{com}^m := \text{com}^m_{\text{allgather}} + \text{com}^m_{\text{bcast}}$, cf. (46) and (49). The formula (50) is used in the following section to investigate the influence of the number of subdomains and coarse elements on the wall-clock time of the computational process. Moreover, it is employed in Section 6 for the prediction of the computational costs for the next time steps after the re-meshing.

5.5. Numerical study of computational costs

We present the study of the efficiency of the two-level hybrid Schwarz preconditioners by a benchmark from [23, 36], namely the rising thermal bubble test case. It simulates the evolution of a warm bubble in a constant potential temperature field. The square computational domain is $\Omega = (0, 1000) \times (0, 1000)$ m, the final physical time $T = 50$ s, and we prescribe the constant mean potential temperature $\bar{\Theta} = 300$ K. The Exner pressure follows from the hydrostatic balance (5) as $P = 1 - g/(c_p \bar{\Theta})x_2$. The initial velocity is equal to zero. Moreover, to the mean flow, we add the potential temperature perturbations

$$\Theta' = \begin{cases} 0 & \text{for } r > r_c, \\ \frac{1}{2}\Theta_c(1 + \cos(\pi r/r_c)) & \text{for } r \leq r_c, \end{cases} \quad (51)$$

where $\Theta_c = 0.5$ K, $r = |x - x_c|$, $x_c = (500, 300)$ m and $r_c = 250$ m. The no-flux boundary condition $\mathbf{v} \cdot \vec{n} = 0$ is prescribed on the whole boundary.

For this numerical study we used a fixed (non-adapted) quasi-uniform triangular grid with $\#\mathcal{T}_{h,m} = 9074$ elements using $p = 3$ polynomial approximation in space and $q = 1$ in time. Therefore, the resulting system \mathbf{A}_m has size $N_m = 725\,920$ and the number of non-zero entries $Z_m = 230\,656\,000$ for all $m = 1, \dots, r$. The time step is chosen adaptively according to (22) with $c_T = 1$, which leads to $r = 1049$ time steps. The stopping condition for the nonlinear algebraic solver (21) was used with $c_A = 10^{-3}$. Therefore, the number of Newton and GMRES iterations is varying for $m = 1, \dots, r$.

We carried out the computations using $M_m = 4, 8, 16, \dots, 512$ subdomains and the coarse mesh $\mathcal{T}_{H,m}$ having M_m , $2M_m$, $4M_m, \dots, 32M_m$ coarse elements (i.e., with the number of splitting $s_m = 1, 2, 4, \dots, 32$, cf. Section 5.3). The number of elements of the local problems is $\#\mathcal{T}_{h,m}^i \approx \#\mathcal{T}_{h,m}/M_m$ for all $i = 1, \dots, M_m$. Table 2 presents the observed quantities in sum over all time levels $m = 1, \dots, r$. Namely, we find the

Table 2: Computational costs for hybrid Schwarz preconditioner for varying number of subdomains M_m , number of elements of the local problem $n_i \approx \#\mathcal{T}_{h,m}$, and coarse mesh elements $n_0 = \#\mathcal{T}_{H,m}$.

M_m	n_i	n_0	it ⁿ	it ^ℓ	F ^A	flops	time(s)	com(s)
4	2268	4	4313	32344	487	2.54E+14	2.59E+04	1.84E+02
4	2268	8	4259	31721	464	2.30E+14	2.53E+04	1.82E+02
4	2268	16	4218	31230	444	2.24E+14	2.48E+04	1.82E+02
4	2268	32	4199	30650	430	2.19E+14	2.44E+04	1.84E+02
4	2268	64	4199	30506	424	2.18E+14	2.39E+04	1.94E+02
4	2268	128	4199	30520	423	2.17E+14	2.40E+04	2.17E+02
M_m	n_i	n_0	it ⁿ	it ^ℓ	F ^A	flops	time(s)	com(s)
8	1134	8	4214	37777	482	8.23E+13	1.32E+04	2.20E+02
8	1134	16	4205	37444	460	8.07E+13	1.30E+04	2.22E+02
8	1134	32	4205	37293	438	7.77E+13	1.30E+04	2.27E+02
8	1134	64	4204	36288	424	7.35E+13	1.29E+04	2.35E+02
8	1134	128	4201	35595	422	7.46E+13	1.28E+04	2.56E+02
8	1134	256	4205	33411	422	7.22E+13	1.26E+04	2.89E+02
M_m	n_i	n_0	it ⁿ	it ^ℓ	F ^A	flops	time(s)	com(s)
16	567	16	4225	34741	457	2.69E+13	6.44E+03	2.09E+02
16	567	32	4212	34439	446	2.68E+13	6.45E+03	2.13E+02
16	567	64	4204	33728	434	2.63E+13	6.52E+03	2.21E+02
16	567	128	4202	33550	429	2.66E+13	6.70E+03	2.44E+02
16	567	256	4201	32701	423	2.72E+13	7.33E+03	2.85E+02
16	567	512	4202	31105	421	4.53E+13	9.11E+03	3.62E+02
M_m	n_i	n_0	it ⁿ	it ^ℓ	F ^A	flops	time(s)	com(s)
32	283	32	4222	33819	467	1.05E+13	3.09E+03	2.12E+02
32	283	64	4202	33274	454	1.05E+13	3.19E+03	2.21E+02
32	283	128	4202	32914	439	9.88E+12	3.53E+03	2.42E+02
32	283	256	4201	32164	432	1.69E+13	4.46E+03	2.84E+02
32	283	512	4203	31110	424	4.28E+13	6.04E+03	3.65E+02
M_m	n_i	n_0	it ⁿ	it ^ℓ	F ^A	flops	time(s)	com(s)
64	141	64	4208	34838	465	3.11E+12	1.28E+03	2.34E+02
64	141	128	4204	34462	450	4.96E+12	1.61E+03	2.57E+02
64	141	256	4205	33665	438	1.36E+13	2.55E+03	3.00E+02
64	141	512	4203	32523	431	4.04E+13	4.70E+03	3.84E+02
M_m	n_i	n_0	it ⁿ	it ^ℓ	F ^A	flops	time(s)	com(s)
128	70	128	4207	36039	460	4.97E+12	1.28E+03	2.72E+02
128	70	256	4205	34975	437	1.44E+13	2.37E+03	3.14E+02
128	70	512	4204	33327	435	4.28E+13	4.69E+03	3.97E+02
M_m	n_i	n_0	it ⁿ	it ^ℓ	F ^A	flops	time(s)	com(s)
256	35	256	4206	36151	451	1.53E+13	2.18E+03	3.28E+02
256	35	512	4204	34242	438	4.40E+13	4.18E+03	4.10E+02
M_m	n_i	n_0	it ⁿ	it ^ℓ	F ^A	flops	time(s)	com(s)
512	17	512	4205	35389	455	4.46E+13	4.53E+03	4.27E+02

$$\begin{aligned}
\text{it}^n &= \sum_{m=1}^r \text{it}_m^n & \text{Newton iterations,} & \text{flops} = \sum_{m=1}^r \text{flops}^m & \text{floating point operations (40),} \\
\text{it}^\ell &= \sum_{m=1}^r \text{it}_m^\ell & \text{GMRES iterations,} & \text{time} = \sum_{m=1}^r \text{time}^m & \text{the wall-clock time of computation (46),} \\
\mathbf{F}^A &= \sum_{m=1}^r \mathbf{F}_m^A & \text{evaluations of matrix } \mathbf{A}_m, & \text{com} = \sum_{m=1}^r \text{com}^m & \text{the wall-clock time of communication (49).}
\end{aligned}$$

We emphasize that time is the real time measured by *MPI_Wtime* function. On the other hand, the communication com represents the estimated wall-clock time for *allgather* and *bcast* by (48a) and (49) with fitted parameters $\alpha_g, \beta_g, \gamma_g, \alpha_b, \beta_b$ and γ_b for data from Section 5.3.3 since we have not enough cores for the maximal number of subdomains $M_m = 512$.

We observe that increasing $\#\mathcal{T}_{H,m}$ reduces the number of GMRES iterations it^ℓ since the finer coarse mesh provides more information. On the other hand, the number of flops is decreasing for increasing $\#\mathcal{T}_{H,m}$ only if the number of coarse elements $\#\mathcal{T}_{H,m}$ is at least several times smaller than the number of elements of the local problems $\#\mathcal{T}_{h,m}^i$. Otherwise, the computational costs of the solution of the coarse problem are non-negligible and they prolong the computation.

Moreover, we find that the minimum in terms of flops ($M_m = \#\mathcal{T}_{H,m} = 64$) does not correspond to the minimum in terms of time ($M_m = \#\mathcal{T}_{H,m} = 128$) since the speed of the computations depends also on the size of the system, see Figure 6. We note that these results are hardware/software dependent. Obviously, the wall-clock time of communication com is increasing for increasing M_m since there are more cores which communicate, and similarly, it is increasing for the size of the coarse problem since the transmitted vectors are longer. Finally, we conclude that the wall-clock time for communication is several times smaller than the time for computation. Nevertheless, it is not negligible.

6. Adaptive domain decomposition

The goal of this section is to present an adaptive domain decomposition technique, which (approximately) solves Problem 4.2. For the generated sequence of systems (35) in time layers $m = 1, \dots, r$, the aim is to choose the number of subdomains M_m and splitting s_m such that the computational costs are minimal. We recall that we consider four contributions to the computational costs: the factorization and substitution of the local and global coarse systems (34).

We employ the computational cost model (50) composed from (46) and (49), where we assume that flops, speed, and com can be estimated from the empirical formulas (41), (44), and (48a), respectively. The parameters c, C, μ, v ,

a, b and \bar{S} from these formulas are evaluated by the standard least square fitting employing the available information from previous time steps which have to be stored during the time marching computation. However, the local problems can be factorized and assembled in parallel. Hence, it is sufficient to store the information only about the largest one, we index it by $i = 1$. The information about the coarse problem has index $i = 0$ in the following.

Let m be the current time step and $\vartheta \geq 2$. For the last ϑ adaptation cycles, we store the following quantities for all $k = 1, \dots, \vartheta$ (in agreement with previous notation)

- N_{m-k} – the size of the global algebraic system (35),
- N_{m-k}^1 – the size of the largest local fine system (34), i.e., $N_{m-k}^1 = \max_{i=1, \dots, M_{m-k}} \dim(S_{m-k,i}^{h,\tau})$,
- N_{m-k}^0 – the size of the global coarse system (34),
- $\text{flops}_{\text{fac}}^{m-k,i}, \text{flops}_{\text{sub}}^{m-k,i}$ – the corresponding values of *flops* for factorization and substitution of local ($i = 1$) and global coarse ($i = 0$) problems given by MUMPS, cf. Section 5.3.1,
- $\text{speed}_{\text{fac}}^{m-k,i}, \text{speed}_{\text{sub}}^{m-k,i}$ – the average *speed* for factorization and substitution of local ($i = 1$) and global coarse ($i = 0$) problems in time step $m - k$,
- F_{m-k}^A – the number of updates of matrix \mathbf{A}_{m-k} in time step $m - k$,
- it_{m-k}^ℓ – the number of GMRES iteration in time step $m - k$ (sum of all Newton steps),
- M_{m-k} – the number of subdomains (= the number of used cores) in time step $m - k$,
- $\text{com}_{\text{allgather}}^{m-k,1}, \text{com}_{\text{bcast}}^{m-k,1}$ – the average wall-clock time of one *allgather* and *bcast* in time step $m - k$.

If a mesh $\mathcal{T}_{h,m}$ is used for several time steps, then we store the previous data only for the last time step executed on $\mathcal{T}_{h,m}$ and ignore the others. We do not emphasise this selection in the notation explicitly.

6.1. Adaptive domain decomposition algorithm

We are ready to introduce the desired adaptive algorithm. As mentioned above, first we set the parameters of empirical formulas using the stored data and them among all candidates of M_m and s_m , we choose those which minimize the computational cost model. Particularly, the algorithm has the following steps:

(A1) fitting of parameters

(A1a) *flops* – in virtue of (41), we define the exponential functions estimating the number of *flops* as

$$\begin{aligned} \mathsf{Fl}_{\text{fac}}^i(N) &:= C_i N^{\mu_0}, & \{C_i, \mu_i\} &= \arg \min_{C, \mu} \sum_{k=1}^{\vartheta} \|\text{flops}_{\text{fac}}^{m-k,i} - C(N_{m-k}^i)^{\mu}\|^2, & i &= 0, 1 \\ \mathsf{Fl}_{\text{sub}}^i(N) &:= c_i N^{\nu_i}, & \{c_i, \nu_i\} &= \arg \min_{c, \nu} \sum_{k=1}^{\vartheta} \|\text{flops}_{\text{sub}}^{m-k,i} - c(N_{m-k}^i)^{\nu}\|^2, & i &= 0, 1. \end{aligned} \quad (52)$$

(A1b) *speed* of computation – in virtue of (44), we define the functions estimating the speed of computations as

$$\begin{aligned} \mathsf{Sp}_{\text{fac}}^i(N) &:= \min(\bar{S}_{\text{fac}}, a_{\text{fac},i} N + b_{\text{fac},i}), & \{a_{\text{fac},i}, b_{\text{fac},i}\} &= \arg \min_{a, b} \sum_{k=1}^{\vartheta} \|\text{speed}_{\text{fac}}^{m-k,i} - a N_{m-k}^i - b\|^2, & (53) \\ \mathsf{Sp}_{\text{sub}}^i(N) &:= \min(\bar{S}_{\text{sub}}, a_{\text{sub},i} N + b_{\text{sub},i}), & \{a_{\text{sub},i}, b_{\text{sub},i}\} &= \arg \min_{a, b} \sum_{k=1}^{\vartheta} \|\text{speed}_{\text{sub}}^{m-k,i} - a N_{m-k}^i - b\|^2, \\ \text{where } \bar{S}_{\text{fac}} &= \max_{k=1, \dots, m-1, i=0,1} \text{speed}_{\text{fac}}^{m-k,i}, & \bar{S}_{\text{sub}} &= \max_{k=1, \dots, m-1, i=0,1} \text{speed}_{\text{sub}}^{m-k,i} & \text{for } i = 0, 1. \end{aligned}$$

(A1c) *number of updates and iterations* – the predictions of the number of updates of matrix \mathbf{A}_{m-k} and the number of GMRES iterations in the Newton solver in the next time step m is difficult to predict, so we use just an average of several last time steps, i.e.,

$$\bar{\mathsf{F}}_m^A := \frac{1}{\vartheta} \sum_{k=1}^{\vartheta} \mathsf{F}_{m-k}^A, \quad \bar{\mathsf{it}}_m^\ell := \frac{1}{\vartheta} \sum_{k=1}^{\vartheta} \mathsf{it}_{m-k}^\ell, \quad (54)$$

(A1d) *communication times* – in virtue of (48a), we define the functions approximating the communication costs (including latency and bandwidth) by

$$\begin{aligned} \text{Com}_{\text{allgather}}(N, P) &= \alpha_g \log_s P + \beta_g N + \gamma_g, \\ \{\alpha_g, \beta_g, \gamma_g\} &= \arg \min_{\alpha, \beta, \gamma} \sum_{k=1}^{\theta} \left\| \alpha \log_2 M_{m-k} + \beta N_{m-k} + \gamma - \text{com}_{\text{allgather}}^{m-k, 1} \right\|^2, \\ \text{Com}_{\text{bcast}}(N, P) &= \alpha_b \log_s P + \beta_b N + \gamma_b, \\ \{\alpha_b, \beta_b, \gamma_b\} &= \arg \min_{\alpha, \beta, \gamma} \sum_{k=1}^{\theta} \left\| \alpha \log_2 M_{m-k} + \beta N_{m-k}^0 + \gamma - \text{com}_{\text{bcast}}^{m-k, 1} \right\|^2, \end{aligned} \quad (55)$$

(A2) let $\mathcal{T}_{h,m}$ and $S_m^{h,\tau}$ be the mesh and functional space generated by the anisotropic hp -mesh adaptation technique, the size of the corresponding algebraic system is $N_m = \dim S_m^{h,\tau}$. For all admissible number of subdomains $M_m = 1, 2, \dots$ and number of splittings $s_m = 1, 2, \dots$, (cf. Remark 6.1)

(A2a) set the corresponding (approximate) sizes of local and global coarse systems

$$N^1 := \frac{N_m}{M_m} \quad \text{and} \quad N^0 := N_m \frac{\#\mathcal{T}_{h,m}}{\#\mathcal{T}_{h,m}} = N_m \frac{s_m M_m}{\#\mathcal{T}_{h,m}}, \quad (56)$$

respectively,

(A2b) in virtue of (45)–(46) and (52)–(54), estimate the wall-clock time for the computation of the next time step as

$$\text{Time}(M_m, s_m) := \bar{F}_m^A \max \left(\frac{\mathsf{Fl}_{\text{fac}}^0(N^0)}{\mathsf{Sp}_{\text{fac}}^0(N^0)}, \frac{\mathsf{Fl}_{\text{fac}}^1(N^1)}{\mathsf{Sp}_{\text{fac}}^1(N^1)} \right) + \bar{it}_m^\ell \left(\frac{\mathsf{Fl}_{\text{sub}}^0(N^0)}{\mathsf{Sp}_{\text{sub}}^0(N^0)} + \frac{\mathsf{Fl}_{\text{sub}}^1(N^1)}{\mathsf{Sp}_{\text{sub}}^1(N^1)} \right), \quad (57)$$

where N^0 and N^1 are given by (56). We recall that the used hybrid method requires the solution of the global coarse system after the solution of the local ones, hence we have to sum both contributions in the second term in (57).

(A2c) in virtue of (49) and (55), estimate the wall-clock time for the communication of the next time step as

$$\text{Com}(M_m, s_m) := \bar{it}_m^\ell \left(\text{Com}_{\text{allgather}}(N^1, M_m) + \text{Com}_{\text{bcast}}(N^0, M_m) \right). \quad (58)$$

(A3) in virtue of (50), (57), and (58), choose the optimal values M_m^{opt} and s_m^{opt} that minimize the predicted computational costs as

$$\{M_m^{\text{opt}}, s_m^{\text{opt}}\} = \arg \min_{M_m=1,2,\dots, s_m=1,2,\dots} (\text{Time}(M_m, s_m) + \text{Com}(M_m, s_m)). \quad (59)$$

Remark 6.1. In practical computations, the terms “all admissible number of subdomains $M_m = 1, 2, \dots$ and number of splittings $s_m = 1, 2, \dots$ ” in step (A2), has natural restrictions. First, M_m is bounded by the number of available cores. In principle, it is possible to use higher number of subdomains M_m than the number of available cores but in this case the computational cost model has to be modified. Moreover, we can assume that each subdomain has at least several elements n^{min} (typically 10, 100, …, depending on the application). From this, we have the restriction

$$M_m \leq M_m^{\text{max}} := \#\mathcal{T}_{h,m} / n^{\text{min}}. \quad (60)$$

Moreover, based on previous considerations and numerical studies, it is natural to restrict to the case when the number of elements of the coarse mesh is lower than the number of elements of the local meshes, i.e.,

$$\#\mathcal{T}_{h,m} = s_m M_m \leq \#\mathcal{T}_{h,m} / M_m \quad \Rightarrow \quad s_m \leq s_m^{\text{max}} := \#\mathcal{T}_{h,m} / M_m^2. \quad (61)$$

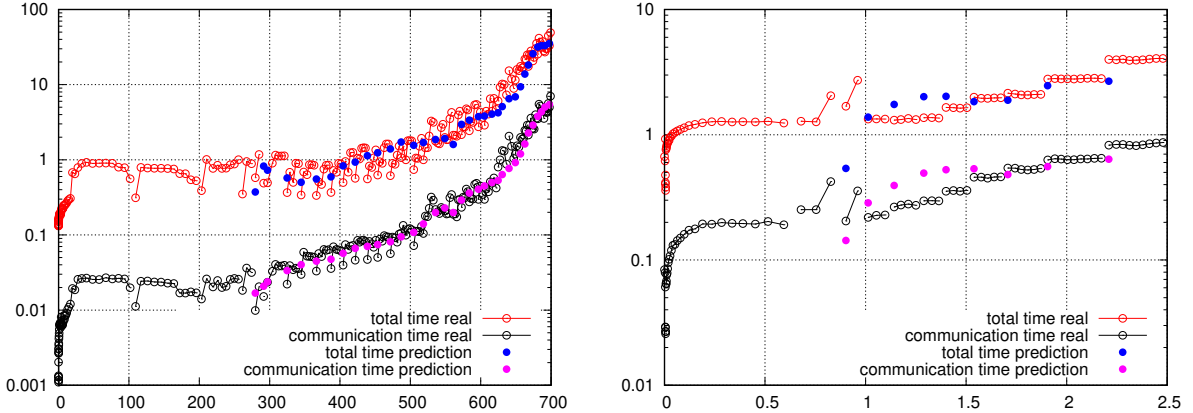


Figure 9: Comparison of the predicted and real wall-clock times (vertical axes) for each time step (the horizontal axis is the physical time); examples from Section 7.1 (left) and Section 7.2 (right).

We note that the algorithm described above cannot be applied in the first ϑ steps. So we have to start the computational process in another way, typically we prescribe the number of subdomains such that the size of a local problem is approximately equal to the given value k_s , thus we put $M_m \approx N_m/k_s$.

Finally, it is necessary to choose the number of time layers ϑ used for the fitting of parameters. The smaller value can better reflect the local in time character of the problem considered but the fitting of parameters is less stable. It is sensitive namely for the speed of computations and wall-time of communications. Therefore, based on numerical experiments, we use the value $\vartheta = 5$ for steps (A1a) and (A1c). On the other hand, we use all the available history for steps (A1b) and (A1d), i.e., $\vartheta = m$.

The quality of the prediction of the computational costs by technique (52)–(58) is shown in Figure 9 which compares the predicted and real wall-clock times for the communications com^m and total time costs^m (computations + communication) for all time steps for examples from Sections 7.1 and 7.2. Each node corresponds to one time step, the filled circles are the predicted times for the next time step, and empty circles are the real times. We observe a reasonably good agreement between the predicted and real times. We recall that the prediction of the computational costs and the subsequent (“optimal”) domain decomposition is carried out only when a new mesh is generated, and it can not be used in a few first time steps.

7. Numerical experiments

We present numerical examples, which demonstrate the efficiency of the proposed adaptive domain decomposition algorithm from Section 6.1. We always run the STDG technique with the anisotropic hp -mesh adaptation described in Section 3.3 with the same parameters, the linear algebraic systems are solved iteratively by GMRES method preconditioned by the two-level hybrid Schwarz preconditioner. Note that their dimension grows during the time stepping. We use three domain decomposition variants of the choice M_m and s_m at time level $m = 1, \dots, r$, cf. Problem 4.2:

FS (Fixed subdomains): The number of subdomains M_m is fixed for all $m = 1, \dots, r$, we set the values $M_m = 10, 20, 30, 50$, and 70 . Additionally, M_m is chosen so that each $\Omega_i, i = 1, \dots, M_m$ has at least 10 elements, otherwise M_m is decreased. The parameter s_m is chosen such that $\#\mathcal{T}_{H,m} \leq \frac{1}{2}\#\mathcal{T}_{h,m}/M_m$, i.e., the number of elements of the coarse grid is at most one half of the number of elements of each subdomain, cf. (61).

FD (Fixed number of degrees of freedom): The number of subdomains M_m is chosen such that each subdomain has approximately the same number of degrees of freedom (unknowns) k_s for all time levels, i.e., $M_m = N_m/k_s$ for all $m = 1, \dots, r$, where $N_m = \dim S_m^{h,\tau}$ is the size of the global system. We use the values $k_s = 4000, 6000, 8000, 10\,000, 12\,000$, and $16\,000$, and we require that $M_m \geq 2$. The parameter s_m is chosen as in FS.

Table 3: Rising thermal bubble, comparison of computation costs for all domain decomposition variants FS, FD, and AD.

variant	M_m	$\#\mathcal{T}_{H,m}$	it^n	it^ℓ	flops	time	com	costs
FS, $M_m = 10$	10	10	752	49122	1.53E+13	1.99E+03	3.18E+01	2.03E+03
FS, $M_m = 20$	20	20	724	48455	5.30E+12	1.53E+03	4.59E+01	1.58E+03
FS, $M_m = 30$	30	30	724	48276	3.15E+12	1.13E+03	6.00E+01	1.19E+03
FS, $M_m = 50$	50	50	716	47810	3.29E+12	1.04E+03	1.59E+02	1.20E+03
FS, $M_m = 70$	70	70	719	47951	5.47E+12	1.31E+03	2.19E+02	1.53E+03
FD, $k_s = 16000$	31	31	622	33903	8.74E+12	2.11E+03	5.26E+01	2.16E+03
FD, $k_s = 12000$	41	41	620	35505	6.07E+12	1.47E+03	7.16E+01	1.54E+03
FD, $k_s = 10000$	49	49	639	38043	4.71E+12	1.30E+03	8.06E+01	1.38E+03
FD, $k_s = 8000$	62	62	639	39381	3.91E+12	1.19E+03	9.53E+01	1.28E+03
FD, $k_s = 6000$	82	82	664	41989	3.15E+12	1.07E+03	1.22E+02	1.19E+03
FD, $k_s = 4000$	123	123	691	46192	4.40E+12	1.18E+03	2.33E+02	1.41E+03
AD, exe 1	65	65	737	50579	2.01E+12	9.68E+02	1.24E+02	1.09E+03
AD, exe 2	65	65	732	49210	2.01E+12	9.62E+02	1.25E+02	1.09E+03
AD, exe 3	53	53	734	49464	1.95E+12	9.67E+02	1.18E+02	1.09E+03
AD, exe 4	53	53	736	50241	2.06E+12	9.81E+02	1.23E+02	1.10E+03
AD, exe 5	65	65	732	49210	2.01E+12	9.61E+02	1.25E+02	1.09E+03
AD, exe 6	56	56	737	50244	1.93E+12	9.51E+02	1.28E+02	1.08E+03
AD, minimum	53	53	732	49210	1.93E+12	9.51E+02	1.18E+02	1.08E+03
AD, average	59	59	734	49824	1.99E+12	9.65E+02	1.24E+02	1.09E+03
AD, maximum	65	65	737	50579	2.06E+12	9.81E+02	1.28E+02	1.10E+03

AD (*adaptive choice*) The number of subdomains M_m and the parameter s_m are chosen adaptively using the algorithm from Section 6.1. Since it depends on the measuring of the wall-clock time during the computational process, which is a system function, we execute the computation with the same setting six times and denote these runs as exe 1, ..., exe 6. For the first 5 steps, we prescribe M_m as in FD with $k_s = 2500$.

In the following, we present the computations for two benchmarks using the types of domain decomposition listed above and compare their computational costs. Similarly as in Section 5.5, we investigate the total number of Newton iterations $it^n = \sum_{m=1}^r it_m^n$, and total number of GMRES iterations $it^\ell = \sum_{m=1}^r it_m^\ell$. However, these quantities have only informative character since the size of the systems \mathbf{A}_m is changing for $m = 1, \dots, r$.

7.1. Rising thermal bubble

We consider the rising thermal bubble test case [23, 36] which simulates the evolution of a warm bubble in a constant potential temperature field. The setting is the same as in Section 5.5, the only difference is that the final physical time is $T = 700$ s, and the mesh is not fixed but the anisotropic hp -mesh adaptation is used. The computational results for all three domain decomposition types FS, FD, and AD are given in Table 3. The columns M_m and $\#\mathcal{T}_{H,m}$ denote the number of subdomains and the number of coarse elements on the last time layer, respectively. The next pair of columns shows the accumulated number of Newton (it^n), and GMRES (it^ℓ) iterations. The next triple of columns shows the number of floating point operations (flops), wall-clock time of computation (time), and wall-clock time of communication (com), the last column contains the total computational costs (costs = time + com), cf. (50). The last three rows are the minimal, average, and maximal values of the AD technique.

We observe that the adaptive setting AD outperforms both other techniques. For FS and FD, there exists a setting giving costs which are not too far from the costs of the AD technique. However, we do not know the optimal setting a priori, it has to be found experimentally, and it is typically case-dependent. On the other hand, AD technique is fully automatic. Additionally, we observe some differences in AD technique with execution exe 1, ..., exe 6. As explained above, the differences are caused by measuring the wall-clock time during the computational process and therefore different domain decomposition is carried out. However, the differences are in the order of a few percents.

Moreover, Figure 10 shows dependence of the accumulated flops(s) = $\sum_{m=1}^s \text{flops}^m$ and costs(s) = $\sum_{m=1}^s \text{costs}^m$ with respect to physical time level $t_s \in [0, T]$, cf. (40) and (50), for selected cases. To better see the differences,

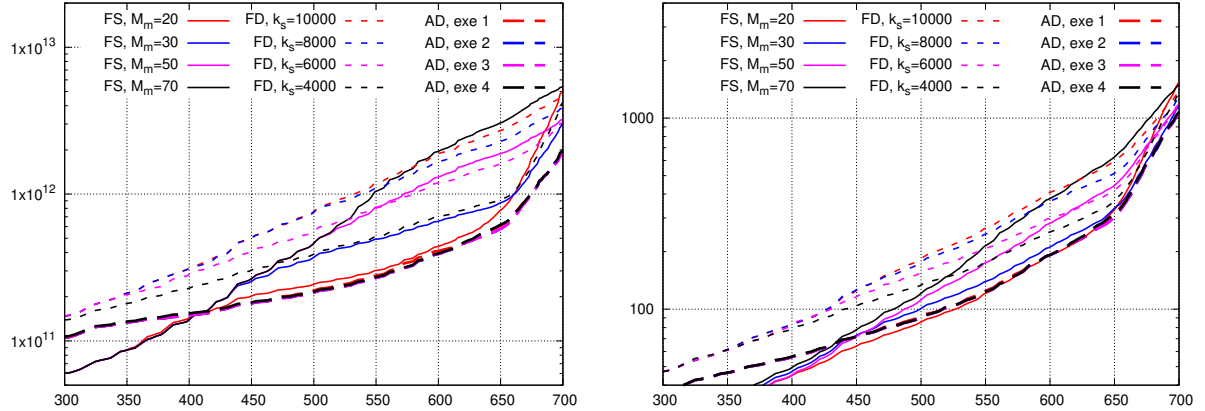


Figure 10: Rising thermal bubble, comparison of all domain decomposition variants FS, FD, and AD, the accumulated flops(s) (left) and total measured time costs(s) (right) for $t_s \in [300, T]$.

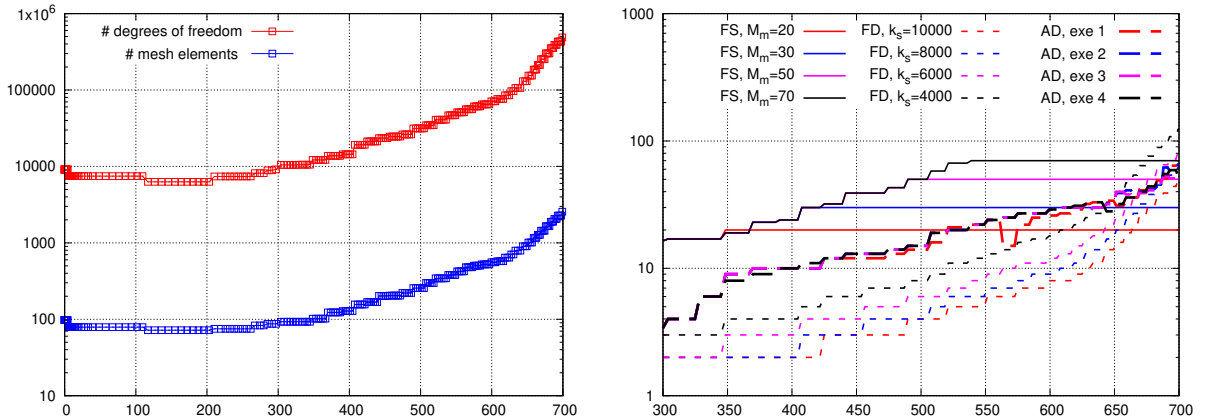


Figure 11: Rising thermal bubble, the number of elements $\#\mathcal{T}_{h,m}$ and degrees of freedom N_m ($= \dim S_m^{h,\tau}$) for each time step $t_m \in [0, T]$ (left), and the number of subdomains M_m for all variants FS, FD, and AD, $t_m \in [300, T]$ (right).

we show only the time interval starting from $t = 300$. Furthermore, Figure 11 shows the increase of the number of elements $\#\mathcal{T}_{h,m}$, the number of degrees of freedom N_m ($= \dim S_m^{h,\tau}$) and the number of subdomains M_m for each time level $t_m \in [0, T]$. The right-hand side graph in Figure 11 illustrates the increase of the number of subdomains M_m . While it is given a priori for FS and FD, the AD technique is automatic, and it gives a slower increase in comparison with the FD choice. Moreover, small differences among executions exe 1, ..., exe 4 are observed. We note that the number of elements and the number of degrees of freedom can also decrease (see the left part of Figure 11 for $t \leq 200$ s) since the mesh optimization process minimizes the number of degrees of freedom while keeping the accuracy below the given tolerance, cf. Section 3.6 and the references therein. For $t \leq 200$ s, the shape of the bubble almost does not change.

Finally, to illustrate the presented adaptive domain decomposition method, Figure 12 shows the snapshots of the time-dependent simulation obtained by the AD technique. We present the distribution of the potential temperature Θ (cf. (4)), the corresponding anisotropic hp -mesh and the domain decomposition (the subdomains are colored) at several time instants. We observe the increasing flow complexity and the corresponding mesh refinement, and increasing number of subdomains M_m for selected $m = 1, \dots, r$.

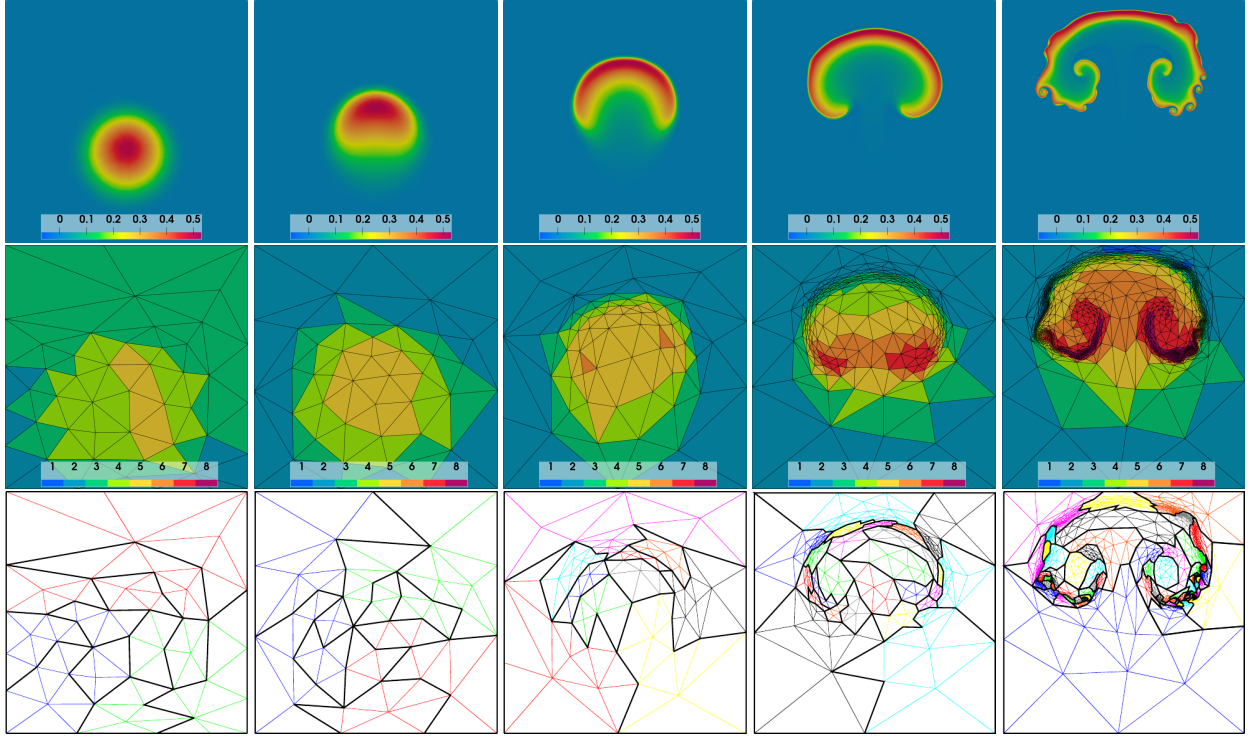


Figure 12: Rising thermal bubble, snapshots of the time-dependent simulation, the distribution of the potential temperature (first row), the anisotropic hp -mesh (second row) and the domain decomposition (third row) at time $t = 100, 250, 400, 550$, and 700 s (from left to right).

7.2. Kelvin-Helmholtz instability

The next example deals with the simulation of the Kelvin-Helmholtz instability, which appears when a velocity difference across the interface between two fluids is presented, cf. [39, 43] for example. Then typical eddies appear, and they are challenging to capture numerically. The problem is described by (1) with no gravity terms.

The computational domain $\Omega = (0, 3) \times (0, 1)$ m is extended periodically in both directions and the final time is $T = 2.5$ s. The initial conditions are given by

$$\begin{cases} \rho = 2, v_1 = -0.5 + \varepsilon, v_2 = \varepsilon, p = 2.5 & \text{if } 0.25 < x_2 < 0.75, \\ \rho = 1, v_1 = 0.5 + \varepsilon, v_2 = \varepsilon, p = 2.5 & \text{if } 0.25 \geq x_2 \text{ or } x_2 \geq 0.75, \end{cases} \quad (62)$$

where we set $\varepsilon = 0.01 \sin(4\pi x_1)$ to trigger the instability. We consider the fluid viscosity $\tilde{\mu} = 2 \cdot 10^{-4} \text{ kg} \cdot \text{m}^{-1} \cdot \text{s}^{-1}$, the heat capacity at constant pressure $c_p = 1005 \text{ J} \cdot \text{kg}^{-1} \cdot \text{K}^{-1}$, the adiabatic Poisson constant $\gamma = 1.4$, and the Prandtl number $Pr = 0.72$.

We compare all three domain decomposition types (FS, FD, and AD) in the same manner as in Section 7.1, the results are given in Table 4. We observe that AD is better than both other techniques in terms of flops, time, and costs. The differences between AD and the optimal choices of FS and FD are not large but, once again, these optimal values have to be found experimentally and differ from the optimal values for examples from Section 7.1. The differences in AD technique with execution exe 1, ..., exe 6 in terms of time are again about a few percents.

Figure 13 shows the dependence of the accumulated flops(s) = $\sum_{m=1}^s \text{flops}^m$ and costs(s) = $\sum_{m=1}^s \text{costs}^m$ with respect to physical time level $t_s \in [0, T]$, cf. (40) and (50), for selected cases. Furthermore, Figure 14 shows the increase of the number of elements $\#\mathcal{T}_{h,m}$, the number of degrees of freedom N_m ($= \dim S_m^{h,\tau}$) and the number of subdomains M_m for each time level $t_m \in [0, T]$. The right-hand side graph in Figure 14 illustrates the increase of the number of subdomains M_m .

Table 4: Kelvin-Helmholtz instability, comparison of computation costs for all domain decomposition variants FS, FD, and AD.

variant	M_m	# $\mathcal{T}_{H,m}$	it ⁿ	it ^ℓ	flops	time	com	costs
FS, $M_m = 10$	10	10	163	5533	7.02E+12	5.01E+02	5.46E+00	5.06E+02
FS, $M_m = 20$	20	20	163	5988	2.54E+12	3.36E+02	8.00E+00	3.44E+02
FS, $M_m = 30$	30	30	163	5868	1.38E+12	2.17E+02	9.10E+00	2.26E+02
FS, $M_m = 50$	50	50	159	5319	6.23E+11	1.52E+02	3.73E+01	1.89E+02
FS, $M_m = 70$	70	70	159	5406	5.32E+11	1.77E+02	4.50E+01	2.22E+02
FD, $k_s = 16000$	26	52	159	4741	3.34E+12	4.41E+02	9.17E+00	4.50E+02
FD, $k_s = 12000$	34	34	158	4740	2.40E+12	3.24E+02	1.16E+01	3.36E+02
FD, $k_s = 10000$	41	41	159	5203	1.92E+12	2.88E+02	1.44E+01	3.02E+02
FD, $k_s = 8000$	51	51	160	5413	1.38E+12	2.45E+02	1.58E+01	2.61E+02
FD, $k_s = 6000$	68	68	161	5508	9.64E+11	1.88E+02	2.00E+01	2.08E+02
FD, $k_s = 4000$	102	102	162	5776	4.47E+11	1.55E+02	2.89E+01	1.84E+02
FD, $k_s = 3000$	136	136	162	5856	4.01E+11	1.36E+02	3.93E+01	1.76E+02
FD, $k_s = 2000$	140	140	159	5610	4.33E+11	1.34E+02	4.71E+01	1.81E+02
AD, exe 1	81	81	159	5567	3.47E+11	1.15E+02	2.95E+01	1.45E+02
AD, exe 2	83	83	159	5518	3.37E+11	1.17E+02	2.95E+01	1.47E+02
AD, exe 3	83	83	159	5501	3.35E+11	1.14E+02	2.95E+01	1.44E+02
AD, exe 4	89	89	159	5571	3.42E+11	1.16E+02	3.11E+01	1.47E+02
AD, exe 5	81	81	159	5567	3.47E+11	1.15E+02	2.94E+01	1.45E+02
AD, exe 6	87	87	159	5522	3.36E+11	1.15E+02	2.95E+01	1.44E+02
AD, minimum	81	81	159	5501	3.35E+11	1.14E+02	2.72E+01	1.42E+02
AD, average	84	84	159	5541	3.41E+11	1.16E+02	2.76E+01	1.43E+02
AD, maximum	89	89	159	5571	3.47E+11	1.17E+02	2.82E+01	1.45E+02

Finally, Figure 15 illustrates the presented adaptive domain decomposition method obtained by the AD technique. We show the distribution of density, the corresponding anisotropic hp -mesh, and the domain decomposition at several time instants. We observe the increasing flow complexity, the corresponding mesh refinement, and the increasing number of subdomains M_m for selected $m = 1, \dots, r$. Remarkably, we observe several symmetries of the solution although the meshes are not strictly symmetric.

8. Conclusion

We have dealt with the adaptive domain decomposition preconditioners for the solution of algebraic systems arising from the space-time discontinuous Galerkin discretization. In particular, we have considered two-level additive and hybrid Schwarz techniques, and proposed a computational cost model involving the wall-clock time of computation and communications of the preconditioner. This model is at the core of an adaptive algorithm which selects the number of subdomains and the number of elements of the coarse mesh in order to minimize the predicted computational costs. The efficiency of the approach was demonstrated on two well-known benchmarks where the adaptive algorithm equipped with the cost model performed better than the optimal versions of the strategies with constant subdomain size and constant number of subdomains, setting of which is even unknown beforehand.

The presented computational cost model can be extended to other types of discretization and preconditioners in a straightforward way. Additionally, the model can be generalised to include other parts of the computational process. This will be the subject of our further research.

Data availability

Data will be made available on request.

Conflict of interest

The authors declare that they have no conflicts of interest.

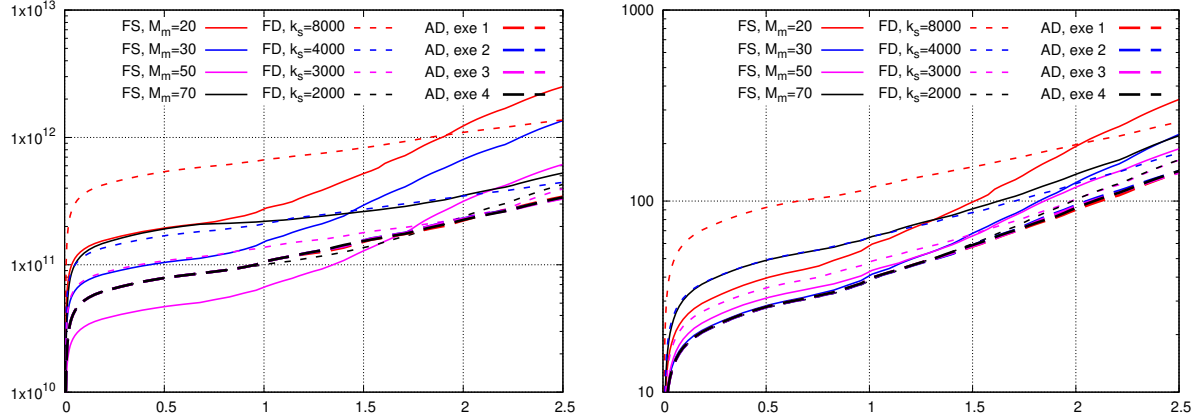


Figure 13: Kelvin-Helmholtz instability, comparison of all domain decomposition variants FS, FD, and AD, the accumulated flops(s) (left) and total measured time costs(s) (right) with respect to physical time $t_s \in [0, T]$.

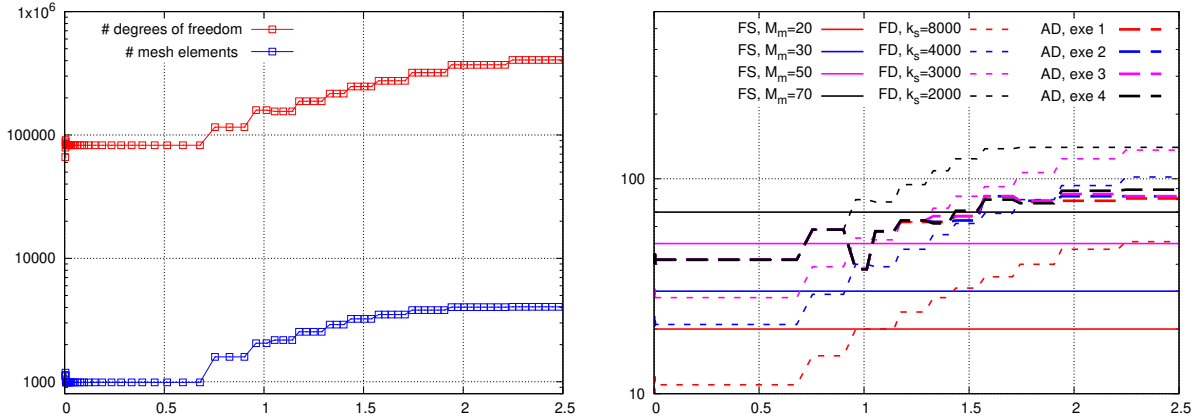


Figure 14: Kelvin-Helmholtz instability, the number of elements $\#\mathcal{T}_{h,m}$ and degree of freedom N_m ($= \dim S_m^{h,\tau}$) for each time step $t_m \in [0, T]$ (left), and the number of subdomains M_m for all variants FS, FD, and AD, $t_m \in [0, T]$ (right).

Acknowledgment

J. Šístek acknowledges the support by grant No. 23-06159S of the Czech Science Foundation and by the Institute of Mathematics of the Czech Academy of Sciences (RVO:67985840). Both authors acknowledge also the membership in the Nečas Center for Mathematical Modeling ncmm.karlin.mff.cuni.cz.

Declaration of generative AI and AI-assisted technologies in the manuscript preparation process.

During the preparation of this work the authors did not use any AI and AI-assisted technologies.

References

- [1] Alauzet, F., Loseille, A., Olivier, G.: Time-accurate multi-scale anisotropic mesh adaptation for unsteady flows in CFD. *J. Comput. Phys.* **373**, 28–63 (2018)
- [2] Alexander, R.: Diagonally implicit Runge–Kutta methods for stiff O.D.E.’s. *SIAM Journal on Numerical Analysis* **14**(6), 1006–1021 (1977)

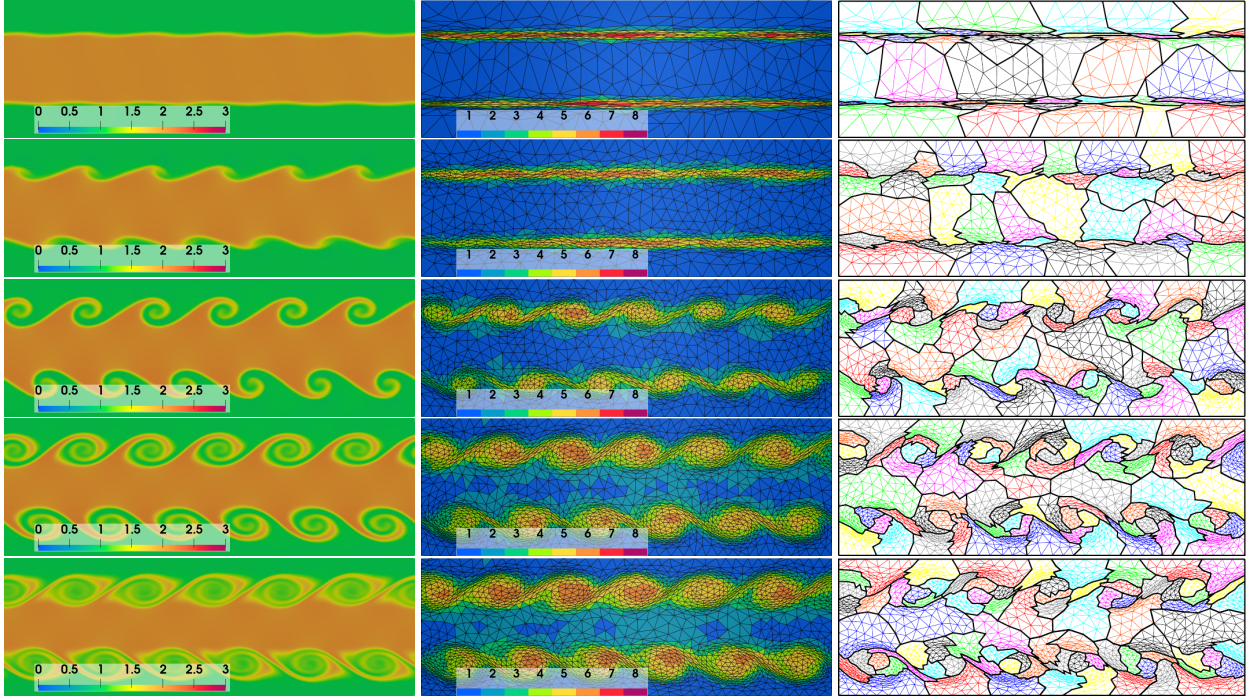


Figure 15: Kelvin-Helmholtz instability, snapshots of the time-dependent simulation, the distribution of the potential temperature (first column), the anisotropic hp -mesh (second column) and the domain decomposition (third column) at time $t = 0.5, 1.0, 1.5, 2.0$, and 2.5 s (from top to bottom).

- [3] Amestoy, P.R., Buttari, A., L'Excellent, J.Y., Mary, T.: Performance and scalability of the block low-rank multifrontal factorization on multicore architectures. *ACM Transactions on Mathematical Software* **45**(1), 2:1–2:26 (2019)
- [4] Amestoya, P.R., Duff, I.S., Koster, J., L'Excellent, J.Y.: A fully asynchronous multifrontal solver using distributed dynamic scheduling. *SIAM J. Mat. Anal. Appl.* **23**(1), 15–42 (2001)
- [5] Antonietti, P.F., Houston, P.: A class of domain decomposition preconditioners for hp -discontinuous Galerkin finite element methods. *J. Sci. Comput.* **46**(1), 124–149 (2011)
- [6] Antonietti, P.F., Houston, P., Smears, I.: A note on optimal spectral bounds for nonoverlapping domain decomposition preconditioners for hp -version discontinuous Galerkin methods. *International Journal of Numerical Analysis and Modeling.* **13**(4), 513–524 (2016)
- [7] Belme, A., Dervieux, A., Alauzet, F.: Time accurate anisotropic goal-oriented mesh adaptation for unsteady flows. *J. Comput. Phys.* **231**(19), 6323–6348 (2012)
- [8] Cai, Y., Wan, J., Kareem, A.: On convergence of implicit Runge-Kutta methods for the incompressible Navier-Stokes equations with unsteady inflow. *J. Comput. Phys.* **523**(113627) (2025)
- [9] Cangiani, A., Dong, Z., Georgoulis, E.H.: Hp-version space-time discontinuous Galerkin methods for parabolic problems on prismatic meshes. *SIAM Journal on Scientific Computing* **39**(4), A1251 – A1279 (2017)
- [10] Cash, J.R.: Diagonally implicit Runge-Kutta formulae with error estimates. *IMA Journal of Applied Mathematics* **24**(3), 293–301 (1979)
- [11] Chan, E., Heimlich, M., Purkayastha, A., van de Geijn, R.: Collective communication: theory, practice, and experience. *Concurrency and Computation: Practice and Experience* **19**(13), 1749–1783 (2007)

- [12] Corallo, D., Dörfler, W., Wieners, C.: Space-time discontinuous Galerkin methods for weak solutions of hyperbolic linear symmetric Friedrichs systems. *Journal of Scientific Computing* **94**(1) (2023)
- [13] Dolean, V., Jolivet, P., Nataf, F.: *An Introduction to Domain Decomposition Methods Algorithms, Theory, and Parallel Implementation*. Society for Industrial and Applied Mathematics (2015)
- [14] Dolejší, V.: Non-hydrostatic mesoscale atmospheric modeling by the anisotropic mesh adaptive discontinuous Galerkin method. *Int. J. Comput. Fluids. Dyn.* **38**(2-3), 81–101 (2024)
- [15] Dolejší, V., Feistauer, M.: *Discontinuous Galerkin Method – Analysis and Applications to Compressible Flow*. Springer Series in Computational Mathematics 48. Springer, Cham (2015)
- [16] Dolejší, V., May, G.: *Anisotropic hp -Mesh Adaptation Methods*. Birkhäuser (2022)
- [17] Dolejší, V., Roskovec, F., Vlasák, M.: Residual based error estimates for the space-time discontinuous Galerkin method applied to the compressible flows. *Comput. Fluids* **117**, 304–324 (2015)
- [18] Dolejší, V., May, G.: An anisotropic hp -mesh adaptation method for time-dependent problems based on interpolation error control. *J. Sci. Comput.* **95**(2) (2023)
- [19] Feng, X., Karashian, O.: Two-level additive Schwarz methods for a discontinuous Galerkin approximation of second order elliptic problems. *SIAM J. Numer. Anal.* **39**, 1343–1365 (2002)
- [20] Frey, P.J., Alauzet, F.: Anisotropic mesh adaptation for CFD computations. *Comput. Methods Appl. Mech. Engrg.* **194**, 5068–5082 (2005)
- [21] Gassner, G., Dumbser, M., Hindenlang, F., Munz, C.D.: Explicit one-step time discretizations for discontinuous Galerkin and finite volume schemes based on local predictors. *J. Comput. Phys.* **230**(11), 4232–4247 (2011)
- [22] Gassner, G., Lörcher, F., Munz, C.D.: A discontinuous Galerkin scheme based on a spacetime expansion. I. Inviscid compressible flow in one space dimension. *J. Sci. Comput.* **32**(2), 175–199 (2007)
- [23] Giraldo, F., Restelli, M.: A study of spectral element and discontinuous Galerkin methods for the Navier–Stokes equations in nonhydrostatic mesoscale atmospheric modeling: Equation sets and test cases. *J. Comput. Phys.* **227**(8), 3849–3877 (2008)
- [24] Habashi, W.G., Dompierre, J., Bourgault, Y., Ait-Ali-Yahia, D., Fortin, M., Vallet, M.G.: Anisotropic mesh adaptation: towards user-independent, mesh-independent and solver-independent CFD. Part I: general principles. *Int. J. Numer. Methods Fluids* **32**(6), 725–744 (2000)
- [25] Hairer, E., Wanner, G.: *Solving Ordinary Differential Equations II, Stiff and Differential-Algebraic Problems*. Springer Verlag (2002)
- [26] Kang, Q., Träff, J.L., Al-Bahrani, R., Agrawal, A., Choudhary, A., keng Liao, W.: Scalable algorithms for MPI intergroup Allgather and Allgatherv. *Parallel Computing* **85**, 220–230 (2019)
- [27] Karakashian, O., Collins, C.: Two-level additive Schwarz methods for discontinuous Galerkin approximations of second-order elliptic problems. *IMA J. Numer. Anal.* **37**, 1800–1830 (2017)
- [28] Karypis, G., Kumar, V.: METIS – A Software Package for Partitioning Unstructured Graphs, Partitioning Meshes, and Computing Fill-Reducing Orderings of Sparse Matrices (2011). <http://glaros.dtc.umn.edu/gkhome/metis/metis/overview>
- [29] Klaij, C.M., van der Vegt, J., der Ven, H.V.: Pseudo-time stepping for space-time discontinuous Galerkin discretizations of the compressible Navier–Stokes equations. *J. Comput. Phys.* **219**(2), 622–643 (2006)
- [30] Klaij, C.M., van der Vegt, J., der Ven, H.V.: Space-time discontinuous Galerkin method for the compressible Navier–Stokes equations. *J. Comput. Phys.* **217**(2), 589–611 (2006)

- [31] Levý, T., May, G.: Towards a robust time-accurate anisotropically adaptive hybridized discontinuous Galerkin method. *Computers and Fluids* **301**(106792) (2025)
- [32] Liesen, J., Strakoš, Z.: *Krylov Subspace Methods: Principles and Analysis*. Clarendon Press, Oxford (2013)
- [33] Message Passing Interface Forum: MPI: A Message-Passing Interface Standard Version 5.0 (2025). URL <https://www.mpi-forum.org/docs/mpi-5.0/mpi50-report.pdf>
- [34] MUMPS: MULTifrontal Massively Parallel sparse direct Solver (2024). mumps-solver.org
- [35] Rhebergen, S., Cockburn, B., van der Vegt, J.J.: A space-time discontinuous Galerkin method for the incompressible Navier-Stokes equations. *Journal of Computational Physics* **233**(1), 339–358 (2013)
- [36] Robert, A.: Bubble convection experiments with a semi-implicit formulation of the Euler equations. *J. Atmos. Sci.* **50**(13), 1865 – 1873 (1993)
- [37] Romeo, F., Dumbser, M., Tavelli, M.: A novel staggered semi-implicit space-time discontinuous Galerkin method for the incompressible Navier-Stokes equations. *Communications on Applied Mathematics and Computation* **3**(4), 607–647 (2021)
- [38] Sauvage, B., Alauzet, F., Dervieux, A.: A space and time fixed point mesh adaptation method. *Journal of Computational Physics* **519** (2024)
- [39] Schroeder, P.W., John, V., Lederer, P.L., Lehrenfeld, C., Lube, G., Schöberl, J.: On reference solutions and the sensitivity of the 2D Kelvin–Helmholtz instability problem. *Computers & Mathematics with Applications* **77**(4), 1010–1028 (2019)
- [40] Segawa, H., Luo, H., Nourgaliev, R.: A Diagonally Implicit Runge–Kutta Method for the Discontinuous Galerkin solutions of the Navier–Stokes Equations, pp. 2011–685. AIAA (2011). <https://arc.aiaa.org/doi/pdf/10.2514/6.2011-685>
- [41] Smears, I., Süli, E.: Discontinuous Galerkin finite element methods for time-dependent Hamilton–Jacobi–Bellman equations with Cordes coefficients. *Numer. Math.* **133**, 141–176 (2016)
- [42] Sudirham, J., van der Vegt, J., van Damme, R.: Space-time discontinuous Galerkin method for advection–diffusion problems on time-dependent domains. *Appl. Numer. Math.* **56**(12), 1491–1518 (2006)
- [43] Svärd, M.: A new Eulerian model for viscous and heat conducting compressible flows. *Physica A: Statistical Mechanics and its Applications* **506**, 350–375 (2018)
- [44] Tavelli, M., Dumbser, M.: Arbitrary high order accurate space-time discontinuous Galerkin finite element schemes on staggered unstructured meshes for linear elasticity. *J. Comput. Phys.* **366**, 386 – 414 (2018)
- [45] Toselli, A., Widlund, O.: Domain decomposition methods—algorithms and theory, *Springer Series in Computational Mathematics*, vol. 34. Springer-Verlag, Berlin (2005)
- [46] Wieners, C.: A space-time discontinuous Galerkin discretization for the linear transport equation. *Computers & Mathematics with Applications* **152**, 294–307 (2023)